

**3D numerical simulation of receptor-mediated leukocyte adhesion  
to surfaces: effects of cell deformability and viscoelasticity**

Damir B. Khismatullin and George A. Truskey

*Department of Biomedical Engineering*

*Duke University, Durham, NC 27708*

(Dated: March 30, 2004)

## Abstract

Computational fluid dynamics is used to investigate the effects of cell deformability and viscoelasticity on receptor-mediated leukocyte adhesion to endothelium or a ligand coated surface in a parallel plate flow chamber. In the three-dimensional numerical code, a leukocyte is modeled as a compound viscoelastic drop (a nucleus covered by a thick layer of cytoplasm). The nucleus, cytoplasm, and extracellular fluid are considered as Newtonian or viscoelastic liquids of high viscosity. The receptor-ligand interaction is incorporated into the code by using the spring-peeling kinetic model under the assumption that leukocyte receptors are located on the tips of cylindrical microvilli distributed over the leukocyte membrane. The code is based on the Volume-of-Fluid method and the Giesekus constitutive equation is implemented in the code to capture viscoelasticity of the cytoplasm and nucleus. Numerical simulations demonstrate the formation and breakup of membrane tethers observed *in vitro* and suggest that the elasticity of the cytoplasm is responsible for a tear-drop shape of rolling leukocytes *in vivo*. When viewed from the top, as normally occurs during shear flow experiments *in vitro*, little or no deformation occurs, a side view shows significant deformation in the contact region. We show that the leukocyte membrane can be extended and disrupted under high shear if the receptor-ligand bonds live in a stressed state for a sufficiently long time. If the shear rate is low, the leukocyte rolls along the surface. The rolling velocity of the viscoelastic cell is smaller than that of the Newtonian cell. This is due to the increased deformability of the viscoelastic cell and, as a result, the decreased torque acting on this cell.

PACS numbers: 87.17.Aa, 87.17.Jj, 82.35.Gh, 83.85.Pt

## I. INTRODUCTION

Leukocytes, also called white blood cells, are an important part of the body's immune system. They protect the body against invading bacteria, parasites, and viruses by killing these microorganisms through phagocytosis (ingestion) and other antigen-specific cytotoxic mechanisms. There exist five different types of leukocytes (neutrophils, eosinophils, basophils, monocytes, and lymphocytes), each of which is designed to fight a specific type of infection<sup>1,2</sup>. These cells are recruited from the circulation to the sites of infection by the process called leukocyte adhesion cascade<sup>3,4</sup>. There are five stages in this process. 1. A leukocyte contacts the activated endothelium of blood vessels near the infected site. Adhesion results if selectins on endothelial cells (ECs) bind to the corresponding receptors on the leukocyte. 2. This interaction mediates rolling of the leukocyte along the endothelium. Otherwise the cell continues to move at the hydrodynamic velocity. 3. Chemoattractant molecules (chemokines)<sup>5</sup> expressed on the activated endothelium trigger the activation of integrins on the leukocyte membrane, which become high-affinity receptors. Selectin binding to its receptor also activates integrin recruitment and affinity changes<sup>6</sup>. Integrins interact with corresponding ligands on the endothelial cells. As a result, rolling of the leukocyte slows down. 4. The leukocyte comes to a stop and attaches firmly to the endothelium by integrin bonds and through the cell activation: the cell is significantly deformed and forms projections, or pseudopods. 5. In the active state, the leukocyte transmigrates across the endothelium and moves toward infection. In some cases leukocytes can adhere via attachment to another leukocyte attached to the endothelium, a process known as secondary adhesion.

Receptor-ligand bonds can be formed if the separation distance between the leukocyte and the endothelium does not exceed the total length of the unstretched receptor and ligand

molecules. The bonds exert a tensile force (often called a bond force) on the cell membrane and cytoskeleton. If the leukocyte is in a passive state, its behavior is dictated by the balance between the bond force and the drag force exerted by blood flow as well as by the balance of the torques due to these forces. Non-specific (electrostatic and van der Waals)<sup>7</sup> and gravitational forces<sup>8</sup> also influence cell-cell adhesion.

Receptor-mediated leukocyte adhesion has been studied theoretically either by analytical or semi-analytical models in which the leukocyte is a 3D rigid cell<sup>9,10</sup> or by numerical 2D models wherein the leukocyte deformability is taken into account<sup>11,12</sup>. Only recently, the adhesive dynamics of non-deformable spherical particles has been examined numerically on the basis of the 3D boundary integral method<sup>13</sup>. In both 2D and 3D models, cell rolling is explained by rapid bond association and dissociation modeled by a kinetic (reaction) equation for the bond density. Two parameters of this equation, the forward reaction rate (on-rate) and the reverse reaction rate (off-rate), define respectively the rates of formation and disruption of receptor-ligand complexes. It is hypothesized that these rates depends exponentially on either the magnitude of the bond force<sup>14</sup> or the difference in length between the stretched and unstretched bonds<sup>15</sup>. In the latter approach, the receptor-ligand complex is assumed to behave in accordance to Hooke's law. Leukocyte rolling becomes possible if the initial on- and off-rates and the spring constant are sufficiently large<sup>16</sup>. In the opposite case, the cell is firmly attached to the adhesive surface.

Leukocytes have a more complex structural organization than other blood cells. In comparison with erythrocytes (red blood cells), white blood cells contain the nucleus, which is characterized by a low deformability, a complex cytoplasm with many organelles, and the cytoskeleton, which ties together the cell membrane, cytoplasm, and nucleus. Leukocytes are less deformable than erythrocytes<sup>17</sup> and conserve their spherical shape when they flow

freely in large blood vessels. However, these cells (with diameter of  $8\ \mu\text{m}$  and more) undergo significant deformation when entering the smallest blood capillaries. *In vivo* experiments<sup>12,18</sup> show that the adherent leukocytes deform to a tear-drop shape during rolling along the endothelium. *In vitro*, leukocytes behave as viscoelastic liquid drops when aspirated into a micropipette<sup>19,20</sup>. The neglect of the leukocyte deformability in the mathematical models is based upon *in vitro* cell adhesion assays<sup>21</sup> which suggest that deformation does not occur at physiological shear stresses. These assays provide only a top view of the adherent leukocytes, unless a more sophisticated technique is used<sup>22</sup>. From the top view, it is very difficult to observe shape changes in the rolling cell, especially near the contact area between the cell and the adhesive surface. Further, the velocities at which leukocytes roll *in vitro*<sup>23,24</sup> and *in vivo*<sup>25</sup> tend to plateau with increasing the wall shear stress. The increased adhesion at higher values of the wall shear stress is due to greater leukocyte deformation<sup>25,26</sup>.

Previous numerical studies on the adhesion of a deformable leukocyte to a substrate treated the cell as a cylindrical body adherent to a planar surface (2D models)<sup>11,12</sup>. Because passive leukocytes are spherical in shape and the adhesion of a cylinder is much stronger than the adhesion of a sphere, these models can not be used for the indirect evaluation of the adhesion parameters and analysis of cell adhesion data. Dong *et al.*<sup>12,27</sup> computed the deformation of a rolling cell under the assumption that the cell is an elastic ring filled by a viscous liquid. Their calculations started from a predefined tear-drop-like shape with a large, flat contact area. Dong *et al.* postulated that the leukocyte deformed to this shape *prior to cell attachment*, while this most likely happens *during cell rolling*<sup>18</sup>. They observed an increase in the contact area and a decrease in the drag coefficients with increasing the wall shear stress. Due to its simplicity, this model can not predict realistic shapes of rolling cells, in particular, a transition from the spherical shape to the tear-drop shape. As will

be shown here, the tear-drop shape is the result of the balance between the drag and bond forces acted on the external part of the cell membrane and an internal tensile force due to elasticity of the cell cytoplasm.

A more appropriate model for leukocyte adhesion has been recently proposed by N'Dri *et al.*<sup>11</sup>. In this model, the leukocyte is a 2D compound Newtonian drop, i.e., it has a core fluid, which corresponds to the nucleus, surrounded by a thick and less viscous layer (the cytoplasm). The shapes of the rolling leukocyte are calculated by the immersed boundary method. N'Dri *et al.* have shown that the cell rheological properties significantly influence the adhesion process, in particular, the presence of the nucleus leads to a decrease in the rolling velocity. However, apart from ignoring the third dimension, the model of N'Dri *et al.* does not include elastic effects and can work only at small cytoplasm-to-fluid viscosity ratios.

In this paper, we report the first results on 3D numerical simulation of receptor-mediated adhesion of a spherical viscoelastic leukocyte to the lower plate in a parallel plate flow chamber. Our code is based on the Volume-of-Fluid method and models a leukocyte as a compound viscoelastic drop. The spring-peeling kinetic model<sup>15</sup> is used to describe the receptor-ligand interaction. Our long-term objective is to develop the numerical code that will be able to model realistically the leukocyte-adhesion cascade both *in vivo* and *in vitro*. In this paper, we examine the effect of cytoplasmic viscoelasticity on the shapes of adherent leukocytes.

## II. THEORETICAL MODEL

Although a passive leukocyte resembles a sphere in shape, its surface membrane is ruffled (Fig. 1). The ruffles, called microvilli<sup>2,28</sup>, produce an excess surface area of the white blood

cell. They protect the cell against the dilation of the membrane bilayer that might occur during deformation of the cell in microvessels. In addition, the microvilli are vital in cell adhesion and rolling. Recent experiments<sup>29</sup> show that the receptors responsible for leukocyte rolling are clustered at the microvilli tips and the leukocyte rolls on the endothelium through the interaction of its microvilli with ECs. As regards the intracellular space, it is possible to distinguish two mechanically different regions of the leukocyte: the nucleus and the cytoplasm. To take into account the presence of both the nucleus and microvilli, we model the leukocyte as a 3D compound viscoelastic drop with elastic rods distributed uniformly or non-uniformly over the membrane (Fig. 2). Each of the rods has receptors at its circular tip. Because the nucleus is more stiff than the cytoplasm<sup>2</sup>, the nuclear viscosity is assumed to be higher than the cytoplasmic viscosity. The cell membrane is supposed to be very thin. It possesses a cortical tension similar to a surface tension at the fluid-fluid interface<sup>30</sup>. Rolling of microvilli-covered cells on surfaces was studied theoretically by Hammer and his co-workers<sup>10,13</sup> under the assumption that microvilli are solid rods. However, micropipette-aspiration experiments<sup>28,31</sup> demonstrate that neutrophil microvilli behave as viscoelastic bodies even at small suction pressures.

The flow domain corresponds to a parallel-plate flow chamber: the cell is suspended in a low-viscosity liquid (extracellular fluid) between the fixed upper and lower plates (Fig. 3). The lower plate is covered uniformly by ligands and the cell is sufficiently close to this plate to form receptor-ligand bonds. Initially the cell body has a spherical shape of radius  $a$  and the extracellular fluid is at rest. The shear flow is created by the pressure gradient  $G$ , which is basically the pressure drop between the left and right boundaries  $P_i - P_o$  divided by the distance between them  $d_x$ . Here the  $x$ -axis is in the flow direction. The pressure gradient grows linearly from zero to some fixed value. No-slip boundary condition is applied

at the lower and upper plates ( $z$ -direction). Periodic boundary conditions are used in the  $x$ - and  $y$ -directions. The velocity field and the leukocyte shape are found from the numerical solution to the Navier-Stokes equations (see the next section).

Receptor-ligand bonds are modeled as Hookean springs with spring constant  $\sigma_b$ . (In this paper, we model adhesion via a single class of receptors.) If the separation distance  $d$  between a microvillus and the plate becomes equal to or less than the unstressed bond length  $l_{b0}$ , the microvillus forms a link with the plate. The link is characterized by the time-dependent number of bonds,  $N_b = N_b(t)$ . It is considered to be broken if the number of bonds becomes zero. We assume that the behavior of the linked microvillus is also described by Hooke's law. Each receptor-ligand bond is in series with a "microvillus spring" characterized by spring constant  $\sigma_{mv}$ . This follows from the fact that the microvillus core is a bundle of parallel actin filaments that extend from the microvillus tip into the cell cytoplasm<sup>2</sup>. The filaments are connected to cytoplasmic tails<sup>32,33</sup> of the receptors located at the tip. In our model, the bonds are aligned in the same direction as the filaments. Therefore the "microvillus spring" (one of the actin filaments) together with the bond form a system of two springs in series, which behaves as an adhesive spring with an effective spring constant

$$\sigma_s = \frac{\sigma_b \sigma_{mv}}{\sigma_b + \sigma_{mv}}. \quad (1)$$

If the number of bonds is  $N_b$ , the microvillus-bond complex represents a system of  $N_b$  adhesive springs in parallel. It is characterized by spring constant  $N_b \sigma_s$ .

We use the modified version of the spring-peeling kinetic model by Dembo *et al.*<sup>15</sup> to find the time-dependent number of bonds for the linked microvillus. In the original spring-peeling model, the bond association and dissociation depend on the standard-state free energy  $\Delta G_b^\circ$

of a stretched or compressed bond spring. Dembo *et al.* defined this energy as

$$\Delta G_b^\circ = \Delta G_0^\circ + E_{pb}, \quad E_{pb} = \sigma_b \frac{(l_b - l_{b0})^2}{2}, \quad (2)$$

where  $\Delta G_0^\circ$  is the standard-state free energy of the unstretched bond spring and  $E_{pb}$  is the elastic potential energy of the bond spring [cf. Eq. (17a) in Ref. 15]. They followed the transition state theory to calculate the forward reaction rate as a function of the bond spring displacement. In particular, they assumed that the standard-state free energy of the transition state had the same form as Eq. (2) but with the different spring constant  $\sigma_{ts}$  called transition state spring constant. Then, the expression for the forward reaction rate is of the form:

$$k_f(l_b) = k_f(l_{b0}) \exp \left[ -\sigma_{ts} \frac{(l_b - l_{b0})^2}{2k_b T} \right] \quad (3)$$

( $k_b T$  is the thermal energy). Since the bond dissociation goes through the same transition state as the bond association according to the transition state theory, this assumption gives the following expression for the reverse reaction rate:

$$k_r(l_b) = k_r(l_{b0}) \exp \left[ (\sigma_b - \sigma_{ts}) \frac{(l_b - l_{b0})^2}{2k_b T} \right]. \quad (4)$$

It should be noted that the functions  $k_f(l_{b0})$  and  $k_r(l_{b0})$  remained unspecified in the Dembo model. The bond surface density  $n_b = n_b(t)$  is found by integrating the kinetic equation<sup>14,15</sup>

$$\frac{dn_b}{dt} = k_f(n_l - n_b)(n_r - n_b) - k_r n_b. \quad (5)$$

Because energy is defined within an additive constant, we can assume that unbound receptor and ligand have zero free energy if they are at rest. To reach the transition state, the receptor and ligand should collide with the total kinetic energy  $E_{kt}$  equal to or more than the Gibbs activation energy  $\Delta G_{ts}$ , which is, according to Dembo *et al.*<sup>15</sup>, a sum of two

parts

$$\Delta G_{ts}^{\circ} = \Delta G_{ts0}^{\circ} + \sigma_{ts} \frac{(l_b - l_{b0})^2}{2}. \quad (6)$$

Here  $\Delta G_{ts0}^{\circ}$  is the Gibbs activation energy for the formation of the unstressed bond. It depends on the unstressed bond length  $l_{b0}$ . In the case of adhesion molecules, the Gibbs activation energy exists due to the electrostatic and other repulsive forces between the molecules. The forward reaction rate

$$k_f(l_{b0}) = k_{f0} \exp\left(-\frac{\Delta G_{ts0}^{\circ}}{k_b T}\right), \quad (7)$$

where  $k_{f0}$  is some constant specific for the given reaction. It can be called “maximal forward reaction rate”.

Dembo *et al.*<sup>15</sup> used Eq. (2) to describe the process of receptor-ligand bond formation under the assumption that  $\Delta G_0^{\circ} = \Delta G_{ts0}^{\circ} > 0$ . They assumed that “the differences between the transition state and the bounded state can be described by a change in the spring constant only”. According to the transition state theory, the process of bond formation from the transition state is thermodynamically favored, i.e., the bounded state energy  $\Delta G_b^{\circ}$  should be always less than the Gibbs activation energy  $\Delta G_{ts}^{\circ}$ . From Eqs. (2) and (6) it follows that receptor-ligand bonds can be formed only if  $\Delta G_0^{\circ} < \Delta G_{ts0}^{\circ}$  and

$$\Delta G_{ts0}^{\circ} - \Delta G_0^{\circ} > (\sigma_b - \sigma_{ts}) \frac{(l_b - l_{b0})^2}{2}. \quad (8)$$

This condition shows that the free energy of the unstressed bond can be negative relative to the unbounded state energy in the most common case of slip bonds, i.e., when  $\sigma_b > \sigma_{ts}$  (cf. below). In our model, we assume that  $\Delta G_0^{\circ} < 0$  and define the standard-state free energy of the bounded state as

$$\Delta G_b^{\circ} = -\Delta G_{b0}^{\circ} + \sigma_b \frac{(l_b - l_{b0})^2}{2}, \quad (9)$$

where  $\Delta G_{b0}^\circ = -\Delta G_0^\circ$  is the magnitude of the standard-state free energy of the unstressed bond. To return to the unbounded state, the bond should have the kinetic energy

$$\begin{aligned} E_{kb} &\geq \Delta G_{ts}^\circ - \Delta G_b^\circ \\ &= \Delta G_{ts0}^\circ + \Delta G_{b0}^\circ - (\sigma_b - \sigma_{ts}) \frac{(l_b - l_{b0})^2}{2}. \end{aligned} \quad (10)$$

The function  $k_r(l_{b0})$  is defined as

$$k_r(l_{b0}) = k_{r0} \exp\left(-\frac{\Delta G_{ts0}^\circ + \Delta G_{b0}^\circ}{k_b T}\right), \quad (11)$$

where the constant  $k_{r0}$  can be called “maximal reverse reaction rate of the unstressed state”.

Both *in vivo*<sup>34</sup> and *in vitro*<sup>24,35</sup> studies on leukocyte rolling have observed the shear threshold phenomenon: cell rolling is prohibited while cell arrest can occur if the wall shear rate is small. If the shear rate grows monotonically, the number of rolling leukocytes increases, reaches the maximum, and then decreases. This phenomenon can be explained by the existence of the transition state for bond formation and disruption. The kinetic energies of many (but not all) colliding receptor and ligand molecules are not enough to overcome the activation barrier if the flow velocity is very small. This means that the number of formed bonds decreases to the minimum when the wall shear rate approaches zero. However, the minimum number of bonds is more than zero due to Brownian motion of molecules and vibration of the experimental setup. On the other hand, bond disruption requires more kinetic energy to overcome the activation barrier than bond formation, i.e., if receptor-ligand bonds are formed at very low shear rate, they have a low probability to be broken by flow and hence have a long lifetime unless the shear rate increases significantly. This is why cell arrest can occur at small flow velocities. If the cell rolls with a nearly constant velocity along a surface, the number of bonds does not change so much: new bonds are formed at the leading edge of the contact region and old bonds are destructed at the trailing edge such

that the total number of bonds is approximately constant at each instant. Cell rolling is impossible if the bond lifetime is very long or very short. In the former case, the number of bonds increases with time and the rolling velocity approaches zero, i.e., the cell is firmly attached to the surface. In the latter case, which occurs at high wall shear rates, the number of bonds decreases with time and the rolling velocity approaches the hydrodynamic velocity, i.e., the cell is detached from the surface. This explains why the number of rolling leukocytes reaches the maximum at moderate wall shear rates.

The existence of so-called “catch” bonds whose lifetime prolonged by the applied force<sup>36</sup> can also contribute to the shear threshold phenomenon. The “catch” behavior of P-selectin / P-selectin glycoprotein ligand-1 (PSGL-1) bonds has been recently observed by the atomic force microscopy<sup>37</sup>. In particular, these bonds behave as catch bonds if the applied force (wall shear stress) is weak but undergo a transition to “slip” bonds (the lifetime of “slip” bonds is diminished with increasing the force) if the applied force is sufficiently strong<sup>37</sup>. It should be noted that Dembo *et al.*<sup>15</sup> were the first who described mathematically “catch” bonds. They concluded that if  $\sigma_b - \sigma_{ts} < 0$ , the receptor-ligand bond behaves as a “catch” bond. The cases  $\sigma_b - \sigma_{ts} = 0$  and  $\sigma_b - \sigma_{ts} > 0$  were classified as “ideal” and “slip” bonds, respectively.

In our theoretical model, each receptor is connected to some actin filament in the microvillus core. if the receptor-ligand bond is formed, the actin filament behave as a Hookean spring, i.e., it changes its potential energy after the bond formation. In this case, the elastic potential energy of the bond spring should be replaced by the elastic potential energy of the microvillus-bond spring. Then, the second terms in the right-hand side of Eqs (6) and (9) are replaced by  $\sigma_{tss}(l_s - l_{mv} - l_{b0})^2/2$  and  $\sigma_s(l_s - l_{mv} - l_{b0})^2/2$ , respectively. Here the constant  $\sigma_{tss}$  is the spring constant of the transition state of the microvillus-bond complex,

$\sigma_s$  is given in Eq. (1),  $l_s$  is the distance between the microvillus base and the plate, which is calculated in the code from the formula:

$$l_s = \sqrt{(x_p - x_{mv})^2 + (y_p - y_{mv})^2 + z_{mv}^2} \quad (12)$$

[see Eqs. (25) and (28)].

Leukocyte-endothelial adhesion depends not only on the kinetics of receptor-ligand bonds but also on the kinetics of receptor extraction from the leukocyte membrane. Leukocyte adhesion molecules usually have three domains<sup>32,33,38,39</sup>: long extracellular domain, hydrophobic membrane-spanning domain, and short cytoplasmic tail/s linked noncovalently to the cytoskeleton. If the pulling force of 100 pN<sup>14,40</sup> is applied to the receptor, the linkages between the membrane-spanning domain and the membrane and between the cytoplasmic tail and the cytoskeleton are broken and the receptor is extracted from the leukocyte surface. In his famous work<sup>14</sup>, Bell pointed out that “pulling receptors out of the membrane may be competitive with breaking ligand-receptor bonds”. Recently, Shao and Hochmuth<sup>40</sup> have showed by using a micropipette aspiration technique that the time and the pulling force needed to extract a receptor are correlated. Mathematically, receptor extraction can be considered as an additional mechanism for the destruction of the microvillus-bond complex, i.e., receptor extraction can be accounted for in the expression for the reverse reaction rate. The simple way to incorporate receptor extraction into the kinetic model is to assume that the microvillus-bond spring has the increased elastic potential energy due to receptor extraction:

$$\Delta G_b^{\circ} = -\Delta G_{b0}^{\circ} + \gamma \sigma_s \frac{(l_s - l_{mv} - l_{b0})^2}{2}, \quad (13)$$

where  $\gamma > 1$  is nondimensional constant which can be called ”correction factor”. There are other reasons, mostly of biochemical character, for an effective decrease in bond lifetime and

hence an increase in  $\gamma$ , including selectin shedding<sup>41</sup> and the increased release of nitric oxide (NO) from activated endothelial cells<sup>42</sup>.

Using the fact that we consider the microvillus-bond spring instead of the bond spring and taking into account Eqs (3), (4), (7), (11), and (13), the forward and reverse reaction rates can be expressed as

$$k_f = k_{f0} \exp\left(-\frac{\Delta G_{ts0}^\circ}{k_b T}\right) \times \exp\left[-\frac{\sigma_{tss}(l-l_{mv}-l_{b0})^2}{2k_b T}\right], \quad (14a)$$

$$k_r = k_{r0} \exp\left(-\frac{\Delta G_{ts0}^\circ + \Delta G_{b0}^\circ}{k_b T}\right) \times \exp\left[\frac{(\gamma\sigma_s - \sigma_{tss})(l-l_{mv}-l_{b0})^2}{2k_b T}\right]. \quad (14b)$$

All living cells behave as viscoelastic materials. The main source for both viscosity and elasticity of the cell is the cell cytoskeleton: a viscoelastic network of actin filaments, intermediate filaments, and microtubules<sup>43,44</sup>. Recent experimental results obtained by the method of two-pointed microrheology indicate that cells should be modeled as “three-dimensional continua rather than cortical shells”<sup>45</sup>, i.e., the cell behavior is dictated by its bulk viscoelasticity but not by its membrane viscoelasticity. Several constitutive models were used to describe the leukocyte viscoelasticity, including standard viscoelastic solid<sup>46</sup>, Maxwell<sup>47</sup>, and power-law fluid models<sup>48</sup>. However, these models are impermissibly simple and, as noted by Drury and Dembo<sup>49</sup>, cannot fully explain all the features of the leukocyte aspiration. Micropipette aspiration experiments show that human neutrophils cannot be described as viscoelastic solids<sup>19,50,51</sup>. They behave as polymeric drops during suction<sup>48,52</sup>. The flow of polymeric liquids is generally described by differential constitutive equations (the Upper-Convected Maxwell, Oldroyd-B, Giesekus, Phan-Thien-Tanner, FENE-P and other models)<sup>53</sup>. In our numerical code, the Giesekus constitutive equation<sup>54</sup> is used to

capture the leukocyte viscoelasticity. This equation is sufficiently simple, yet gives good predictions about the stress growth in startup shear flow and the steady-shear-rate viscosity of polymeric liquids<sup>53,55,56</sup>. (The startup shear flow is just considered in our simulations.) Our work is the first attempt to use a more realistic rheological model for modeling leukocyte deformation.

The Giesekus model is the generalization of the Oldroyd-B model and can describe both the elastic and shear thinning behavior of polymeric liquids. It is derived from a kinetic theory<sup>54</sup> and takes into account two different phases of a polymeric liquid: solvent phase and polymer phase. The solvent phase is a Newtonian liquid of small viscosity. The polymer phase is a viscoelastic fluid of high viscosity. For a living cell, the solvent phase is the cell cytosol and the polymer phase is the cell cytoskeleton (all proteins that form the cytoskeleton represent polymers). Mathematically, the Giesekus constitutive equation is for the extra stress tensor  $\mathbf{T}$ , which is the polymer contribution to the shear stress: the shear stress tensor  $\tau = 2\mu^s\mathbf{S} + \mathbf{T}$ , where  $2\mu^s\mathbf{S}$  is the Newtonian (solvent) part of the stress tensor. The Giesekus model has the form<sup>53</sup>

$$\lambda_1 \left[ \frac{\partial \mathbf{T}}{\partial t} + (\mathbf{u} \cdot \nabla) \mathbf{T} - (\nabla \mathbf{u}) \mathbf{T} - \mathbf{T} (\nabla \mathbf{u} \nabla)^\dagger + \kappa \mathbf{T}^2 \right] + \mathbf{T} = 2\mu^p \mathbf{S}. \quad (15)$$

Here  $\lambda_1$  is the relaxation time,  $\mu^p$  the polymer viscosity,  $\kappa$  the Giesekus nonlinear parameter (it is often expressed in terms of the nondimensional mobility factor  $\alpha$  as  $\kappa = \alpha/\mu^p$ )<sup>53</sup>. The term  $(\mathbf{u} \cdot \nabla) \mathbf{T}$  is the advection term of the constitutive equation,  $\mathbf{T}^2$  the nonlinear term, and  $(\nabla \mathbf{u}) \mathbf{T} - \mathbf{T} (\nabla \mathbf{u} \nabla)^\dagger$  the contravariant term of the constitutive equation. If  $\kappa = 0$ , the Giesekus model is reduced to the Oldroyd-B model. If  $\kappa = \mu_p = 0$ , the Upper-Convected Maxwell (UCM) model is obtained.

### III. NUMERICAL IMPLEMENTATION

The 3D numerical simulation of leukocyte-surface adhesion under flow is carried out by our own incompressible CFD code in which the modified Volume-Of-Fluid (VOF) method is used for tracking shapes of the cell over time. The full numerical algorithm of the code is as follows:

**Step 0:** Initialization (base flow, initial profile of the leukocyte, microvilli distribution).

#### Cycle in time

**Step 1:** Piecewise-Linear Interface Calculation (PLIC): reconstruction of the leukocyte shape.

**Step 2:** Advection of the microvilli and interfaces:  $\mathbf{x}_{mv}^{(n)} \rightarrow \mathbf{x}_{mv}^{(n+1)}$ ,  $C_1^{(n)} \rightarrow C_1^{(n+1)}$ ,  $C_2^{(n)} \rightarrow C_2^{(n+1)}$ .

**Step 3:** Calculation of surface forces by the Continuous Surface Force (CSF) method.

**Step 4:** Calculation of the bond force.

**Step 5:** Calculation of an intermediate velocity using the semi-implicit factorized scheme for the Navier-Stokes equations:  $\mathbf{u}^{(n)} \rightarrow \mathbf{u}^*$ .

**Step 6:** Solving the Poisson equation for pressure by the multigrid method.

**Step 7:** Correction of the intermediate velocity by the pressure term:  $\mathbf{u}^* \rightarrow \mathbf{u}^{(n+1)}$ .

**Step 8:** Calculation of the extra stress tensor using the semi-implicit factorized scheme for the Giesekus constitutive equation:  $\mathbf{T}^{(n)} \rightarrow \mathbf{T}^{(n+1)}$ .

**End of Cycle**

### A. Leukocyte shape reconstruction

In the classical VOF method<sup>57–59</sup>, the interface between two fluids is reconstructed from a concentration (or volume fraction) function that takes the value 1 in the first fluid and the value 0 in the second fluid. The interface passes through the computational cells in which the concentration function is between 0 and 1. This function of time and coordinates is advected by the velocity field according to a simple partial differential equation (called topological equation). Because we model a leukocyte as a compound drop, there are three different fluids (the nucleus, cytoplasm, and extracellular fluid) and two interfaces (the nucleus-cytoplasm interface and the membrane). Leukocyte shapes are, therefore, tracked by two concentration functions,  $C_1 = C_1(t, \mathbf{x})$  and  $C_2 = C_2(t, \mathbf{x})$ , responsible for the nucleus and cytoplasm, respectively. Here  $\mathbf{x} = (x, y, z)$  is a position vector. In particular,

$$C_1(t, \mathbf{x}) = \begin{cases} 1 & \text{inside the nucleus (fluid 1),} \\ 0 & \text{outside} \end{cases} \quad (16a)$$

$$C_2(t, \mathbf{x}) = \begin{cases} 1 & \text{inside the cytoplasm (fluid 2)} \\ 0 & \text{outside} \end{cases} \quad (16b)$$

In the extracellular fluid (region outside the leukocyte),  $C_1(t, \mathbf{x}) = C_2(t, \mathbf{x}) = 0$ . Then, the nucleus-cytoplasm interface consists of points  $(x, y, z)$  in which

$$0 < C_1(t, \mathbf{x}) < 1, \quad C_1(t, \mathbf{x}) + C_2(t, \mathbf{x}) = 1. \quad (17)$$

The points that belong to the leukocyte membrane satisfy the following conditions:

$$0 < C_2(t, \mathbf{x}) < 1, \quad C_1(t, \mathbf{x}) = 0. \quad (18)$$

The concentration functions change with time according to the topological equation:

$$\frac{\partial C}{\partial t} + \mathbf{u} \cdot \nabla C = 0, \quad C = C_1 \text{ or } C_2, \quad (19)$$

where  $\mathbf{u} = (u, v, w)$  is the velocity vector and  $\nabla C = (\partial C/\partial x, \partial C/\partial y, \partial C/\partial z)$  is the gradient of  $C$ .

The leukocyte shape is reconstructed from the concentration functions by the Piecewise-Linear Interface Calculation (PLIC) method<sup>57,60</sup>. If condition (17) or (18) is satisfied in a given grid cell, the grid cell is supposed to be divided by a planar surface into two parts. In the case of (17), the first and second parts belong to the nucleus and cytoplasm and have the volumes equal to  $V_g C_1(t, \mathbf{x}_g)$  and  $V_g[1 - C_1(t, \mathbf{x}_g)]$ , respectively, where  $V_g = \Delta x \Delta y \Delta z$  is the volume of the grid cell and  $\mathbf{x}_g = (x_g, y_g, z_g)$  the position vector to the grid cell center. In the case of (18), the volumes of the first part (cytoplasm) and of the second part (extracellular fluid) are  $V_g C_2(t, \mathbf{x}_g)$  and  $V_g[1 - C_2(t, \mathbf{x}_g)]$ . The normal to the planar surface is given by either  $\mathbf{n}_1$  or  $\mathbf{n}_2$  estimated by the CSF method (see below). After reconstruction of the leukocyte shape, its deformation under flow is modeled by Eq. (19). In our code, a Lagrangian form of this equation is used<sup>57</sup>.

## B. Continuous surface forces

One of the advantages of the VOF method is that velocity fields in immiscible fluids are found by solving one set of Navier-Stokes equations with averaged values of mass density and shear viscosity  $[\rho(t, \mathbf{x})$  and  $\mu^s(t, \mathbf{x})]$  based on the concentration function. In our problem, three different fluids are present. The averaged values are, therefore, given by

$$\begin{aligned} \psi(t, \mathbf{x}) = & C_1(t, \mathbf{x})\psi_n + C_2(t, \mathbf{x})\psi_{cp} + [1 - C_1(t, \mathbf{x}) \\ & - C_2(t, \mathbf{x})]\psi_{ec}, \quad \psi = \rho, \mu^s, \mu^p, \lambda_1, \text{ or } \kappa \end{aligned} \quad (20)$$

where the indexes “ $n$ ”, “ $cp$ ” and “ $ec$ ” indicate the nucleus, cytoplasm, and extracellular fluid, respectively. Because of this averaging, the boundary conditions at the interfaces

can not be applied directly and, therefore, all surface forces are included in the Navier-Stokes equations as body forces which act on the fluids within transition regions between the nucleus and the cytoplasm and between the cytoplasm and the extracellular fluid. In our model, we do not consider surface rheology of the cell membrane. The cortical tension at the membrane is identical, in terms of mathematical description, to the surface tension at the interface between two fluids. The cortical tension and the surface tension at the nucleus-cytoplasm interface are implemented into the Navier-Stokes equations by using the Continuous Surface Force (CSF) method by Brackbill *et al.*<sup>61</sup> In the case when this method is applied to the compound drop problem, the discontinuities in the concentration functions present at the interfaces are smoothed artificially by the interpolation function (mollifier)  $S(\mathbf{x}' - \mathbf{x}; h)$ , which decreases monotonically with the distance from the interface. In our code, the mollifier is of the form<sup>62</sup>

$$S(\mathbf{x}' - \mathbf{x}; h) = \begin{cases} A \left[ 1 - \frac{\|\mathbf{x}' - \mathbf{x}\|^2}{4h^2} \right]^4 & \text{if } \|\mathbf{x}' - \mathbf{x}\| < 2h, \\ 0 & \text{if } \|\mathbf{x}' - \mathbf{x}\| \geq 2h. \end{cases} \quad (21)$$

The mollified concentration functions  $c_1(t, \mathbf{x})$  and  $c_2(t, \mathbf{x})$  are convoluted as

$$c_1(t, \mathbf{x}) = \int_V C_1(t, \mathbf{x}') S(\mathbf{x}' - \mathbf{x}; h) dx' dy' dz' \quad (22a)$$

$$c_2(t, \mathbf{x}) = \int_V C_2(t, \mathbf{x}') S(\mathbf{x}' - \mathbf{x}; h) dx' dy' dz', \quad (22b)$$

where  $h$  and  $V$  are the thickness and volume of the transition regions and  $\mathbf{x}' = (x', y', z')$ . These functions are used to find the outward normal vectors  $\mathbf{n}_1 = \mathbf{n}_1(t, \mathbf{x})$  and  $\mathbf{n}_2 = \mathbf{n}_2(t, \mathbf{x})$  to and mean curvatures  $\kappa_1 = \kappa_1(t, \mathbf{x})$  and  $\kappa_2 = \kappa_2(t, \mathbf{x})$  of the nucleus-cytoplasm interface

and membrane:

$$\mathbf{n}_1 = -\frac{\nabla c_1}{\|\nabla c_1\|}, \quad \mathbf{n}_2 = -\frac{\nabla c_2}{\|\nabla c_2\|}, \quad (23a)$$

$$\kappa_1 = \nabla \cdot \mathbf{n}_1 - [\mathbf{n}_1(\mathbf{n}_1 \cdot \nabla)] \cdot \mathbf{n}_1,$$

$$\kappa_2 = \nabla \cdot \mathbf{n}_2 - [\mathbf{n}_2(\mathbf{n}_2 \cdot \nabla)] \cdot \mathbf{n}_2 \quad (23b)$$

The forces due to surface tension at the nucleus-cytoplasm interface and due to cortical tension [ $\mathbf{F}_{nc} = \mathbf{F}_{nc}(t, \mathbf{x})$  and  $\mathbf{F}_m = \mathbf{F}_m(t, \mathbf{x})$ ] are approximated as

$$\mathbf{F}_{nc} = -\sigma_{nc}\kappa_1\|\nabla c_1\|\mathbf{n}_1, \quad \mathbf{F}_m = -\sigma_m\kappa_2\|\nabla c_2\|\mathbf{n}_2. \quad (24)$$

Here  $\nabla \cdot \mathbf{n} = \partial n_x/\partial x + \partial n_y/\partial y + \partial n_z/\partial z$  is the divergence of  $\mathbf{n}$ ,  $\sigma_{nc}$  the nucleus-cytoplasm surface tension coefficient, and  $\sigma_m$  the cortical tension coefficient.

### C. Receptor-ligand interaction

We assume that  $N_{mv}$  cylindrical microvilli of radius  $r_{mv}$  and length  $l_{mv}$  are distributed uniformly or nonuniformly over the cell membrane. Initially, we introduce the receptor and ligand surface densities  $n_r$  and  $n_l$ , the spring constants ( $\sigma_{tss}$ ,  $\sigma_b$ , and  $\sigma_{mv}$ ), the thermal energy  $k_bT$ , and the parameters  $\gamma$ ,  $k_{f0}$ ,  $k_{r0}$ ,  $\Delta G_{ts0}^\circ$ ,  $\Delta G_{b0}^\circ$ ,  $l_{mv}$ , and  $l_{b0}$ . The initial position of each microvillus  $\mathbf{x}_{mv} = (x_{mv}, y_{mv}, z_{mv})$  is calculated using spherical coordinates centered on the cell<sup>10</sup>. Because the microvilli are attached to the cell membrane, they are advected, together with the points of the membrane, by the velocity field. The new position of each microvillus is defined as

$$\begin{aligned} x_{mv}^{(n)} &= x_{mv} + \frac{\delta x_{mv}}{\Delta x} u_r + \left(1 - \frac{\delta x_{mv}}{\Delta x}\right) u_l, \\ y_{mv}^{(n)} &= y_{mv} + \frac{\delta y_{mv}}{\Delta y} v_r + \left(1 - \frac{\delta y_{mv}}{\Delta y}\right) v_l, \\ z_{mv}^{(n)} &= z_{mv} + \frac{\delta z_{mv}}{\Delta z} w_r + \left(1 - \frac{\delta z_{mv}}{\Delta z}\right) w_l, \end{aligned} \quad (25)$$

where  $\Delta x$ ,  $\Delta y$  and  $\Delta z$  are the dimensions of the grid cell wherein the microvillus axis intersects the membrane,  $\delta x_{mv} = x_{mv} - x_l$ ,  $\delta y_{mv} = y_{mv} - y_l$  and  $\delta z_{mv} = z_{mv} - z_l$  are the differences between the microvillus coordinates and the coordinates of the left-near-bottom vertex of the grid cell,  $u_l$  and  $u_r$  are  $x$ -components of the velocity vector at the left and right sides of the grid cell,  $v_l$  and  $v_r$  are  $y$ -components of the velocity vector at the near and far sides of the grid cell, and  $w_l$  and  $w_r$  are  $z$ -components of the velocity vector at the bottom and top sides of the grid cell.

All microvilli are oriented normal to the cell membrane. To find the position of the microvillus tip  $\mathbf{x}_{tip} = (x_{tip}, y_{tip}, z_{tip})$ , we use the normal vector  $\mathbf{n}_2(t, \mathbf{x}_g)$  calculated by the CSF method in the grid cell considered in the advection procedure:

$$\mathbf{x}_{tip} = \mathbf{x}_{mv} + l_{mv}\mathbf{n}_2(t, \mathbf{x}_g). \quad (26)$$

Receptors at the tip are oriented in the same direction as the microvillus. Therefore, if the  $z$ -component of the normal vector  $n_{2z}$  is negative, we calculate the distance between the microvillus tip and the lower plate  $d$  as

$$d = -z_{tip}/n_{2z}. \quad (27)$$

If this distance is equal to or less than the unstressed bond length  $l_{b0}$ , a receptor-ligand bond is created, i.e., the microvillus forms a link with the plate. It is assumed that receptors can interact with ligands inside a circular region of radius  $r_{mv}$  centered on the plate at  $(x_p, y_p, 0)$ , where

$$x_p = x_{tip} + n_{2x}d, \quad y_p = y_{tip} + n_{2y}d. \quad (28)$$

These coordinates are memorized in the code up to the instant when the microvillus is detached from the plate.

The bond surface density  $n_b = n_b(t)$  is calculated from Eqs. (5) and (14). Because the receptor-ligand interaction area is  $\pi r_{mv}^2$ , the number of bonds is

$$N_b = \text{trunc}(\pi r_{mv}^2 n_b), \quad (29)$$

where “trunc” denotes truncation to the integer. If  $N_b = 0$ , the link is considered to be broken, i.e., the microvillus is detached from the plate. Otherwise, we calculate the microvillus-bond force  $\mathbf{F}_{mv} = \mathbf{F}_{mv}(t, \mathbf{x}_g)$  (the force that acts on the leukocyte membrane due to the receptor-ligand interaction at the microvillus tip) inside the grid cell where the microvillus is originated. The  $x$ -,  $y$ -, and  $z$ -components of this force are as follows:

$$F_{mv}^x = n_b k_s \left( \frac{l_{mv} + l_{b0}}{l} - 1 \right) (x_{mv} - x_p) \|\nabla c_2\|, \quad (30a)$$

$$F_{mv}^y = n_b k_s \left( \frac{l_{mv} + l_{b0}}{l} - 1 \right) (y_{mv} - y_p) \|\nabla c_2\|, \quad (30b)$$

$$F_{mv}^z = n_b k_s \left( \frac{l_{mv} + l_{b0}}{l} - 1 \right) z_{mv} \|\nabla c_2\|. \quad (30c)$$

Because the bond force acts on the leukocyte surface, it is transformed to the body force by multiplying  $\|\nabla c_2\|$  just as the force due to cortical tension in (24). If the grid cell has several microvilli, the total bond force  $\mathbf{F}_b = \mathbf{F}_b(x, \mathbf{x}_g)$  that act in this computational cell is taken to equal the sum of microvilli-bond forces:

$$\mathbf{F}_b = \sum_{i=1}^{N_g} \mathbf{F}_{mv}^{(i)}, \quad (31)$$

where  $N_g$  is the number of microvilli in the grid cell. This force is substituted into the Navier-Stokes equations.

#### D. Navier-Stokes equations

The continuity and Navier-Stokes equations

$$\nabla \cdot \mathbf{u} = 0, \quad (32)$$

$$\begin{aligned} \rho \left( \frac{\partial \mathbf{u}}{\partial t} + \mathbf{u} \cdot \nabla \mathbf{u} \right) = & -\nabla p + \nabla \cdot (\mathbf{T} + 2\mu^s \mathbf{S}) \\ & + \rho \mathbf{g} + \mathbf{F}_{nc} + \mathbf{F}_m + \mathbf{F}_b. \end{aligned} \quad (33)$$

are solved by Chorin's projection method<sup>63</sup>. Here  $\rho$  and  $\mu^s$  are the averaged values of the mass density and solvent viscosity defined in (20),  $p = p(t, \mathbf{x})$  is the pressure,  $\mathbf{g} = (0, 0, -g)$  is the acceleration due to gravity,  $\mathbf{F}_{nc}$ ,  $\mathbf{F}_m$ , and  $\mathbf{F}_b$  are surface forces calculated in (24) and (31). The tensors

$$\mathbf{S} = \frac{1}{2} (\nabla \mathbf{u} + \nabla \mathbf{u}^\dagger) \quad (34)$$

and  $\mathbf{T}$  are the rate-of-strain and extra stress tensors. The extra stress tensor is due to the leukocyte viscoelasticity (see below). In the Newtonian case, all components of this tensor are zeros.

The governing equations are discretized on a staggered Marker-and-Cell (MAC) grid<sup>64</sup>, i.e., the pressure  $p$ , concentration functions  $C_1$  and  $C_2$ , and diagonal extra-stress components  $T_{xx}$ ,  $T_{yy}$  and  $T_{zz}$  are defined in the center of a grid cell, but the velocity components  $u$ ,  $v$  and  $w$  and the non-diagonal extra-stress components  $T_{xy}$ ,  $T_{xz}$  and  $T_{yz}$  are defined on its sides and edges, respectively (Fig. 4). The finite-difference spatial derivatives are then calculated by centered differences over a single mesh spacing, where possible.

To avoid the problem of viscous diffusion instability, which imposes strict restrictions on the time step size in the case of small Reynolds number, we use the semi-implicit scheme for the intermediate velocity  $\mathbf{u}^*$  (calculated in the first part of the projection method). This scheme is proven to be unconditionally stable<sup>65,66</sup>. In the semi-implicit scheme, the diffusion

terms (unmixed second derivatives of the velocity) are implicit. It is precisely these terms that are responsible for viscous diffusion instability<sup>64</sup>. All other parts of the Navier-Stokes equation are left explicit. Diffusion is due to the Stokes operator  $A$ :

$$\mathbf{A}\mathbf{u}^* = 2\nabla \cdot (\mu^s \mathbf{S}) = \mathbf{D} + \mathbf{E}. \quad (35)$$

The vectors  $\mathbf{D} = (D_x, D_y, D_z)$  and  $\mathbf{E} = 2\nabla \cdot (\mu^s \mathbf{S}) - \mathbf{D}$ , where

$$D_x = \frac{\partial}{\partial x} \left( \mu^s \frac{\partial u^*}{\partial x} \right) + \nabla \cdot (\mu^s \nabla u^*), \quad (36a)$$

$$D_y = \frac{\partial}{\partial y} \left( \mu^s \frac{\partial v^*}{\partial y} \right) + \nabla \cdot (\mu^s \nabla v^*), \quad (36b)$$

$$D_z = \frac{\partial}{\partial z} \left( \mu^s \frac{\partial w^*}{\partial z} \right) + \nabla \cdot (\mu^s \nabla w^*), \quad (36c)$$

can be considered as the diffusion and dilatation terms of  $\mathbf{A}\mathbf{u}^*$ . (Note that the intermediate velocity field is not divergence-free.) The diffusion term is treated implicitly, but the dilatation term is explicit.

To solve the resulting semi-implicit equations, we use a factorization technique<sup>66,67</sup>. This technique is also applied to the constitutive equation for leukocyte viscoelasticity. The Poisson equation for pressure (the second part of the projection method) is solved by the multigrid method adapted to the variable mesh, with the two-color Gauss-Seidel method for iteration and the Galerkin method for coarse grid correction<sup>68</sup>.

The major problem with numerical integration of differential constitutive equations is the numerical instability caused by the advection term. This instability is generated if the advection term is treated explicitly<sup>69</sup>. As a result, explicit schemes can be used only for very small relaxation times. The only way to avoid the advection instability is to treat the advection term of the constitutive equation implicitly. In this case, as follows from the von Neumann stability analysis, the numerical scheme will be unconditionally stable, i.e., it can be used for any value of the relaxation time.

We have developed the semi-implicit scheme for the Giesekus constitutive equation [see Eq. (15)]. According to this scheme, the advection term and the last term in the left-hand side of the equation are in the implicit part, but the contravariant and nonlinear terms are treated explicitly. The Giesekus constitutive equation in the semi-implicit scheme can be expressed at time step  $n + 1$  as

$$\left\{ \lambda_1 + \Delta t + \lambda_1 \Delta t \left[ u^{(n+1)} \frac{\partial}{\partial x} + \lambda_1 v^{(n+1)} \frac{\partial}{\partial y} + \lambda w^{(n+1)} \frac{\partial}{\partial z} \right] \right\} \mathbf{T}^{(n+1)} = \text{explicit terms.} \quad (37)$$

Although the semi-implicit scheme is unconditionally stable on the MAC grid, it is very time-consuming to solve directly the resulting discretized equations because the direct solution requires the inversion of a large sparse matrix. The effective way to invert the left-hand side of the equations is using a factorization technique<sup>67</sup> according to which Eq. (37) is replaced by

$$\begin{aligned} & (\lambda_1 + \Delta t) \left[ 1 + \frac{\lambda_1 \Delta t}{\lambda_1 + \Delta t} \frac{\partial}{\partial x} u^{(n+1)} \right] \left[ 1 + \frac{\lambda_1 \Delta t}{\lambda_1 + \Delta t} v^{(n+1)} \frac{\partial}{\partial y} \right] \\ & \times \left[ 1 + \frac{\lambda_1 \Delta t}{\lambda_1 + \Delta t} w^{(n+1)} \frac{\partial}{\partial z} \right] \mathbf{T}^{(n+1)} = \text{explicit terms.} \end{aligned} \quad (38)$$

If  $\lambda_1$  is much greater than  $\Delta t$ , the error of the above factorization is of order  $(\|\mathbf{u}\|_{max} \Delta t)^2$ . It becomes smaller if  $\lambda_1$  is of order  $\Delta t$ . The inversion of the factorized LHS requires solving only three tridiagonal matrices, thereby reducing computation time and memory.

#### IV. RESULTS AND DISCUSSION

In the simulations discussed here, a leukocyte resides in a Newtonian extracellular fluid of viscosity  $\mu_{ec}^s = 0.001 \text{ Pa}\cdot\text{s} = 1 \text{ cP}$  and mass density  $\rho_{ec} = 1000 \text{ kg/m}^3$ . We ignore the effect of gravity on leukocyte-plate adhesion, i.e., we assume that the nuclear and cytoplasmic

densities are equal to the extracellular fluid density:  $\rho_n = \rho_{cp} = \rho_{ec}$ . The cortical tension  $\sigma_m = 30 \text{ pN}/\mu\text{m}$  is in the range of experimental values for neutrophils<sup>30,48</sup>. The surface tension at the nucleus-cytoplasm interface is not measured yet, so we select  $\sigma_{nc} = \sigma_m$ . The microvillus radius  $r_{mv} = 0.1 \mu\text{m}$  (Refs 14,28). The bond spring constant  $\sigma_b = 5300 \text{ pN}/\mu\text{m}$  is a measured value for P-selectin/PSGL-1 bonds<sup>70</sup>. The unstressed length of a bond  $l_{b0} = 10 \text{ nm}$  (Ref. 71) and the thermal energy  $k_b T = 4 \times 10^{-21} \text{ J}$  corresponds to the absolute temperature  $T \approx 290 \text{ K}$ .

Leukocyte of two types are considered: a neutrophil and a monocyte. The neutrophil radius  $a = 4 \mu\text{m}$  (Ref. 72) and the nucleus occupies 21% of the cell body volume (Ref. 46). The neutrophil adhesion cascade occurs in postcapillary venules as a part of the inflammatory response<sup>4</sup>. Since the diameter of these vessels ranges from 7 to 30  $\mu\text{m}$  (Refs. 73,74), the distance between plates  $d_z$  is taken to be 16  $\mu\text{m}$ . The size of the computational box  $d_x \times d_y \times d_z = 40 \mu\text{m} \times 40 \mu\text{m} \times 16 \mu\text{m}$ . The adhesion dynamics of the neutrophil is characterized by the number of microvilli  $N_{mv} = 1089$  (microvilli concentration is decreased with  $z$ ), the forward and reverse rate constants  $k_{f0} = 10^{-11} \text{ m}^2/\text{s}$  and  $k_{r0} = 1 \text{ s}^{-1}$  (Ref. 75), spring constant of the transition state  $\sigma_{tss} = 160 \text{ pN}/\mu\text{m}$ , ‘‘correction factor’’  $\gamma = 2.0625$ , and microvillus spring constant  $\sigma_{mv} = 340 \text{ pN}/\mu\text{m}$  (as shown by Park *et al.*<sup>76</sup>, microvilli of neutrophils rolling in a parallel-plate flow chamber behave as elastic bodies with spring constant ranged from 152 to 1340  $\text{pN}/\mu\text{m}$ ). The surface densities of receptors and ligands are large ( $n_r$  and  $n_l$  change from  $5 \times 10^{14} \text{ m}^{-2}$  to  $5 \times 10^{15} \text{ m}^{-2}$  and from  $5 \times 10^{15} \text{ m}^{-2}$  and  $5 \times 10^{16} \text{ m}^{-2}$ , respectively), because of receptor clustering on the microvilli tips<sup>14,29</sup>. For simplicity, we assume that the energy thresholds  $\Delta G_{ts0}^\circ = \Delta G_{b0}^\circ = 0 \text{ J}$ . It is necessary to say that current experimental methods are unable to measure the time course of bond density and therefore the kinetic parameters are defined from the changes in the fraction of adherent cells in the flow chamber

with time<sup>77</sup>. A novel micropipette-aspiration method for measuring the adhesion probability per contact proposed by Chesla *et al.*<sup>75</sup> is also unable to extract the information about  $k_{f0}$  because the contact area  $A_c$  remains undefined. The measured value of  $A_c k_{f0}$  is of the order of  $10^{-7} \mu\text{m}^4/\text{s}$  (Ref. 75). We consider a higher value of  $k_{f0}$  to decrease the computation time.

Monocytes are large leukocytes: their diameter is between 10 to 14  $\mu\text{m}$  (Refs. 78). They play important roles in the immune response of the human body<sup>1</sup> and in the atherosclerosis<sup>79,80</sup>. We consider a monocyte of radius 6.5  $\mu\text{m}$  with 20% of its body volume belonging to the nucleus. In the case of the monocyte, the computational box is 50  $\mu\text{m} \times 50 \mu\text{m} \times 50 \mu\text{m}$ , so the distance between plates  $d_z = 50 \mu\text{m}$ , which is greater than that in the case of the neutrophil. The number of microvilli is 252. They are distributed uniformly over the cell membrane. The  $N_{mv} = 1236$  in the simulations of cell rolling. The microvillus spring constant  $\sigma_{mv} = 210 \text{ pN}/\mu\text{m}$ , spring constant of the transition state  $\sigma_{tss} = 100 \text{ pN}/\mu\text{m}$ , the “correction factor”  $\gamma = 3$ . The surface densities of receptors and ligands  $n_r = 1.5 \times 10^{15} \text{ m}^{-2}$  and  $n_l = 3 \times 10^{15} \text{ m}^{-2}$ , so that there are 47 receptors on the microvillus tip. The forward reaction rate constant  $k_{f0} = 10^{-10} \text{ m}^2/\text{s}$ , the energy thresholds  $\Delta G_{ts0}^\circ = \Delta G_{b0}^\circ = 0 \text{ J}$ . The reverse reaction rate constant  $k_{r0}$  changes from 0.1 to 1000  $\text{s}^{-1}$ .

For the given geometry, the plane Poiseuille flow is formed as a result of the pressure gradient  $G = -dp/dx$ . The wall shear stress (WSS)  $\tau_w$ , wall shear rate (WSR)  $\dot{\gamma}_w$ , and maximal (centerline) velocity of the flow  $U_{max}$  are then calculated as

$$\tau_w = \frac{Gd_z}{2}, \quad \dot{\gamma}_w = \frac{Gd_z}{2\mu_{ec}^s}, \quad U_{max} = \frac{Gd_z^2}{8\mu_{ec}^s} = \frac{\dot{\gamma}_w d_z}{4}. \quad (39)$$

The pressure gradient is selected in such a way as to have  $\tau_w = 4 \text{ Pa}$  and  $\dot{\gamma}_w = 4000 \text{ s}^{-1}$ . We choose such a large shear stress to clearly show the effect of deformation. We also consider the case  $\tau_w = 0.4 \text{ Pa}$  and  $\dot{\gamma}_w = 400 \text{ s}^{-1}$  in the simulations of monocyte rolling.

A variety of the values for the unstressed microvillus length  $l_{mv}$ , solvent viscosities of the cytoplasm and nucleus  $\mu_{cp}^s$  and  $\mu_n^s$ , and polymer viscosities of the cytoplasm and nucleus  $\mu_{cp}^p$  and  $\mu_n^p$  are considered in the paper. When the leukocyte is treated as a viscoelastic cell, the cytoplasmic relaxation time  $\lambda_{1m} = 0.176$  s. This value was extracted from the parameters of a standard viscoelastic solid model of the leukocyte<sup>46</sup>. The nucleus relaxation time  $\lambda_{1n} = 0.200$  s. The case  $\lambda_{1cp} = \lambda_{1n} = 0.010$  s is also discussed. The Giesekus nonlinear parameter  $\kappa$  is taken to be zero (both for the nucleus and cytoplasm) in all the simulations. It should be noted that leukocyte deformation is dictated by its bulk viscoelasticity during the whole time of its contact with the plate. The leukocyte can behave as a Newtonian drop only if the time after the first contact is much more than the relaxation time provided that no changes in flow conditions and in bond association/dissociation occur during this time. However, cell adhesion is not a static process. The surface density of bonds changes with time, microvilli attach to and detach from the plate. Every receptor-ligand interaction and microvillus attachment/detachment cause an immediate elastic response of the cell.

In the code, the governing equations are in the nondimensional form. The characteristic time, length, and density are defined as

$$t_* = \frac{\mu_{ec}^s d_z}{\sigma_m}, \quad l_* = d_z, \quad \rho_* = \rho_{ec}. \quad (40)$$

### A. Neutrophil motion and adhesion: validation of computational approach

To validate the computational analysis, we compared the speed and deformation of a Newtonian drop with analytical results and choose the mesh which is dense enough to capture cell deformation. Figure 5 shows a side view ( $y = 20 \mu\text{m}$ ) of the velocity field and of the neutrophil shape when it moves in the central flow stream. Here the neutrophil is

a Newtonian fluid for which cytoplasmic and nuclear viscosities are  $\mu_{cp}^s = 0.001$  Pa·s and  $\mu_n^s = 0.1$  Pa·s. Initially, the cell center is located at  $(x_c, y_c, z_c) = (8 \mu\text{m}, 20 \mu\text{m}, 8 \mu\text{m})$ . Because the cell is far from the plates, the presence of microvilli on the cell membrane is disregarded. The simulation is performed on  $128 \times 128 \times 64$  mesh with time step  $\Delta t = 0.01 \mu\text{s}$ .

During the neutrophil motion in the parabolic velocity field, its front is elongated in the form of paraboloid and its back is flattened. The forward end of erythrocytes is also deformed to a paraboloidal shape in Poiseuille flow, especially if the distance between walls is small<sup>81</sup>. The deformed shape is reminiscent of the three-lobed shape of a Newtonian droplet immersed in Poiseuille flow between infinite parallel plates<sup>82</sup>. From the analytical study by Nadim and Stone<sup>82</sup> it follows that if the nucleus and cytoplasm together are considered as a single Newtonian liquid, the leading-order deformation of the initially-spherical cells located at the centerline of the flow is described by the formula

$$r = a + \frac{\mu_{ec}^s \dot{\gamma}_w a^3}{\sigma_m d_z} \frac{10 + 11\lambda}{8(1 + \lambda)} f(\theta, \phi). \quad (41)$$

Here  $\lambda$  is the ratio of the cell viscosity

$$\mu_c = (1 - \alpha)\mu_{cp} + \alpha\mu_n \quad (42)$$

( $\alpha = 0.21$  is the volume fraction of the nucleus) to the extracellular fluid viscosity  $\mu_{ec}^s$ ,  $(r, \theta, \phi)$  are the coordinates of the cell surface in a spherical coordinate system with the origin located at the cell center,  $\theta$  and  $\phi$  are measured respectively from the  $z$ -axis (side view) and the  $x$ -axis (top view). Note that if the cell is Newtonian,  $\mu_{cp} = \mu_{cp}^s$  and  $\mu_n = \mu_n^s$ . The shape correction function [see Eq. (5.10b) in Ref. 82]

$$f(\theta, \phi) = \frac{\cos \theta}{5} (\cos^2 \theta + \sin^2 \theta \sin^2 \phi - 4 \sin^2 \theta \cos^2 \phi). \quad (43)$$

is responsible for a three-lobed shape of this cell. It should be noted that Eq. (41) is valid if the cortical tension forces are larger than the viscous forces (of the flow) trying to deform the cell. The formation of the concave regions near the cell front is not observed if the cell is modeled as a compound Newtonian droplet, as seen in Fig. 5. The more viscous nucleus (with non-zero surface tension between the nucleus and cytoplasm) is slightly elongated in the direction perpendicular to the flow and retards the bending deformation of the neutrophil. As a result, the cell is deformed to a paraboloidal shape. Although the measured values for the neutrophil viscosity are much higher<sup>19,48,52</sup> than those used in the simulation, the similar deformation is expected, based on Eq. (41), for a compound cell of higher viscosity.

Another important result of the paper by Nadim and Stone<sup>82</sup> is that the translational velocity of the droplet is always less than the flow velocity. In the case of plane Poiseuille flow, the translational velocity of the leukocyte  $U_c$  can be found from

$$U_c(z) = U(z) - \frac{\lambda U_{max}}{2 + 3\lambda} \left( \frac{2a}{d_z} \right)^2, \quad (44)$$

where

$$U(z) = U_{max} \left[ 1 - \left( \frac{2z - d_z}{d_z} \right)^2 \right] \quad (45)$$

is the velocity of Poiseuille flow. In the Newtonian case, the averaged viscosity of the cell  $\mu_c^s$  can be calculated from Eq. (42). This gives  $\mu_c^s = 0.02179$  Pa·s, i.e.,  $\lambda = \mu_c^s / \mu_{ec}^2 = 21.79$ . The centerline velocity  $U_{max} = U(d_z/2) = 16$   $\mu\text{m}/\text{ms}$ . If the cell is at the centerline, its translational velocity should be  $U_c(d_z/2) \approx 14.7$   $\mu\text{m}/\text{ms}$ . Indeed, the difference in the  $x$ -coordinate of the cell center between  $t = 0.9$  ms and  $t = 0$  ms (the fourth and first pictures in Fig. 5) divided by the time is  $(21.2 - 8)/0.9$   $\mu\text{m}/\text{ms} \approx 14.67$   $\mu\text{m}/\text{ms}$ . The velocity field and interface advection are therefore calculated correctly in the numerical code.

Figure 6 shows the deformation of the adherent neutrophil. The cell is characterized by

the cytoplasmic viscosity  $\mu_{cp}^s = 0.1$  Pa·s and nuclear viscosity  $\mu_n^s = 1$  Pa·s. It also has 1089 microvilli of length  $l_{mv} = 0.09$   $\mu\text{m}$ . The center of the cell is located at (10  $\mu\text{m}$ , 25  $\mu\text{m}$ , 4.1  $\mu\text{m}$ ). The remaining parameters are the same as in the previous case. Initially, the neutrophil is attached to the plate by one microvillus. The shear-induced drag force causes the translational motion of the cell in the flow direction which in its turn stretches the microvillus-bond spring. The spring extension is also associated with the drag torque. As long as the vertical component of the spring force is small, the cell rotates clockwise due to the drag torque. This rotation magnifies briefly the number of linked microvilli. However, the effect of the drag torque on the spring extension is much smaller than that of the drag force because the cell viscosity is low in the simulation. When the microvillus-bond spring is stretched, it produces a pulling force on the cell membrane. As a result, the cell undergoes significant deformation near the contact area. In particular, the adherent part of the cell membrane is stretched in the direction of the spring force (Fig. 6). Such elongation of the cell membrane extends the effective length of the microvillus (in this case, a complex of linked microvilli). It can be considered as “cell body contribution to the microvillus extension”. An analogous deformation of the adherent cell has been observed in 2-D numerical simulations by N’Dri *et al.*<sup>11</sup>. The third and fourth pictures of Fig. 6 show the formation of the concave region (membrane bending) just above the adhesive contact. This is the precursor of a large extension and subsequent breakup of the cell membrane. If the averaged cell viscosity decreases by a factor of 10 or more, the more pronounced deformation is observed. The deformed shape of the Newtonian cell of low viscosity is reminiscent of a bow (not shown here). Note that mesh refinement ( $128 \times 128 \times 128$  and  $256 \times 256 \times 64$ ) does not affect the leukocyte shape.

## B. Monocyte adhesion: high wall shear rate

The numerical simulation of monocyte adhesion to a lower plate in a parallel-plate flow chamber, under the assumption that the cell is Newtonian, is illustrated in Figs. 7 and 8. The cytoplasmic and nuclear viscosities of the monocyte are 0.1 Pa·s and 1 Pa·s, respectively. 252 microvilli of length  $0.09 \mu\text{m}$  are distributed uniformly over the membrane. The reverse reaction rate constant  $k_{r0} = 100 \text{ s}^{-1}$ . The wall shear stress  $\tau_w$  and wall shear rate  $\dot{\gamma}_w$  are again 4 Pa and  $4000 \text{ s}^{-1}$ . Initially, one microvillus of the cell forms a link with the plate. This (and subsequent) simulation is performed on  $64 \times 64 \times 128$  mesh with time step  $0.1 \mu\text{s}$ . The initial position of the cell center  $(x_c, y_c, z_c) = (10 \mu\text{m}, 25 \mu\text{m}, 6.6 \mu\text{m})$ .

Again, the microvillus, stretched due to the translational motion of the monocyte, exerts a pulling force on the monocyte membrane. As seen in Fig. 7 (pictures on the left), the membrane is extended with the formation of the concave region above the contact area. This behavior is identical to that observed in the previous case. Note that the membrane extension is now driven by one linked microvillus. When the extended portion of the monocyte membrane reaches a critical length, it is quickly elongated and finally disrupted (the pictures on the right of Fig. 7). The fast elongation and breakup of the cell membrane are similar to the formation and breakup of tethers from the neutrophil microvilli observed *in vitro*<sup>28,83</sup>. Therefore, it can be called “cell body contribution to tether pulling”.

Figure 8 compares *in vitro* images of tether pulling and breakup during neutrophil rolling along the adhesive plate of the parallel-plate flow chamber with the numerical images (top view of the cell shown in Fig. 7). There are definite similarities between the experimental data and numerical simulation: the membrane extension is followed by the fast elongation and breakup. The breakup time is much shorter in the numerical calculation than in the

experiment because of the difference in the WSR (in the experiment,  $\dot{\gamma}_w = 150 \text{ s}^{-1}$ ). As pointed out by Schmidtke and Diamond<sup>83</sup>, the tether growth rate increases significantly as the WSR is increased. The *in vitro* images show a longer tether than the numerical images because the latter display the cell body deformation only (the stretched microvillus is not shown in the numerical images). Tether pulling is also contributed from the viscous extension (lipid flow) of the microvillus. It can proceed if the pulling forces exerted on receptor-ligand bonds are sufficiently strong to peel off the microvillus membrane from the cytoskeleton<sup>28,84</sup>. In the present work, the viscous response of the microvillus is not considered.

The process of the microvillus extension and tether pulling resulted from (a) cell body deformation and (b) microvillus deformation. This is confirmed experimentally: “the process of tether formation caused a slight teardrop-shaped deformation of the neutrophil”<sup>83</sup>. (From the top view, it is impossible to observe the concave region, which should be formed before the tether formation, and therefore only the tear-drop shape can be predicted. As will be shown later, a long tether is not formed if the cell has indeed a tear-drop shape). The calculation of the microvillus spring constant from the tether length is inappropriate if the effect of cell body deformation on this length is not included. Because the unstressed microvillus length is small in the simulation ( $l_{mv} = 0.09 \mu\text{m}$ ), we expect that there will be no large difference between the present simulation and the simulation with zero microvillus length. In this connection the numerical images in Figs. 7 and 8 show the process of tether formation from neutrophils treated by latrunculin A<sup>85</sup>. This toxin destroys the actin cytoskeleton of the cell, i.e., it causes microvilli to disappear. As a result, cells treated with latrunculin A have a smooth surface (see Fig. 4 in Ref. 85). Also, the destruction of the actin cytoskeleton leads to decreasing the cell elasticity. Our simulations are consistent with the hypothesis that the formation of long tethers is associated with the local cytoskeleton

failure where the cell membrane separates from the underlying actin cytoskeleton<sup>28,84,85</sup>. After such a failure, the attached portion of the cell undergoes purely viscous deformation. As will be shown later, long tethers are not formed if the cell elasticity is taken into account. On the whole, tether formation and breakup is an indicator of leukocyte weakness. The “healthy” leukocytes have a strong yet flexible cytoskeleton which protects them against a loss of their material. Under *in vitro* conditions, the cells are inevitably weakened because they are “uprooted from the organism”. Therefore, the tether formation seems to be a rare phenomenon *in vivo*.

From rheological point of view, the normal living cells behave as viscoelastic fluids, mainly due to the cytoskeleton<sup>44</sup>. The elastic effects on the deformation and adhesion of monocytes are shown in Figs. 9 and 10. In this simulation, elasticities of the monocyte cytoplasm and nucleus are characterized by the relaxation times 0.176 s (Ref. 46) and 0.200 s. The solvent viscosities of the cytoplasm and nucleus are equal to the viscosity of the extracellular fluid:  $\mu_{cp}^s = \mu_n^s = \mu_{ec}^s = 0.001$  Pa·s. The cytoplasm and nucleus have the polymer viscosities  $\mu_{cp}^p = 3.528$  Pa·s and  $\mu_n^p = 10$  Pa·s, so that their total viscosities  $\mu_{cp} = \mu_{cp}^s + \mu_{cp}^p = 3.529$  Pa·s and  $\mu_n = \mu_n^s + \mu_n^p = 10.001$  Pa·s, respectively. The total viscosity of the cell is calculated from Eq. (42). The reverse reaction rate constant  $k_{r0} = 10$  s<sup>-1</sup>. The remaining parameters are the same as in the previous case.

There is no tendency for the formation of long tethers from the viscoelastic cell. Instead of the local deformation near the contact area which finally leads to tether pulling, the “elastic adaptation” of the viscoelastic cell to shear stresses is observed (Fig. 9). To decrease the pulling force on the cell membrane, this cell is elongated in the direction parallel to the microvillus-bond spring. The large concave region responsible for membrane pulling is not formed. As seen in Fig. 9, the deformed shape of the viscoelastic cell is exactly the tear-

drop shape to which rolling leukocytes are deformed *in vivo*[Fig. 11(a)]. The wall shear stress is sufficiently high and hence the pulling force due to the microvillus-bond spring extension is sufficiently strong to extend the adherent part of the monocyte membrane. This monocyte is finally detached from the plate and only a small fragment of the cell membrane is left on the plate (Fig. 10). The computed tear-drop shape of the viscoelastic cell is mainly due to elastic normal stresses inside this cell. Most of the polymeric liquids are characterized by the positive first normal stress difference  $N_1 = T_{xx} - T_{zz}$  (the difference between the elastic normal stresses parallel and perpendicular to the flow direction)<sup>53</sup>. Such a difference creates extra tension in the flow direction for each fluid element of a viscoelastic fluid, which in its turn is responsible for many prominent viscoelastic effects, including rod climbing and polymer extrusion<sup>53</sup>. The Giesekus constitutive equation<sup>53</sup> used in our numerical simulations also gives the positive normal stress difference. In the case of leukocyte-plate adhesion under shear, extra tension in the flow direction produced by  $N_1$  is responsible for the “elastic adaptation” of the cell. In particular, it creates the force against the formation of the concave region. The existence of intracellular extra tension in the flow direction can be explained by alignment of actin microfilaments along the flow (much as happens with polymeric liquids<sup>53</sup>).

The experimentally observed tear-drop shape of rolling leukocytes is due to the leukocyte viscoelasticity. It can not be obtained if the leukocyte is treated as a Newtonian cell. Indeed, viscoelastic cells are deformed to a tear-drop shape for a wide range of polymer viscosities [Fig. 11(b) and 12(a,b)], whereas Newtonian cells have a more complicated shape with a concave region as discussed before. Our simulations also show that viscoelastic cells are more deformed than Newtonian ones even at high polymer viscosities. This is because of the stress growth in startup shear flow<sup>53</sup>: if the relaxation time of a viscoelastic cell is

not zero, the shear stresses and hence the apparent viscosity of the cell grow with time from zero-shear-rate to steady-shear-rate values according to  $1 - \exp(-t/\lambda_1)$ . A decrease in viscoelastic cell deformation is expected when  $t \sim \lambda_1$ . It is observed in micropipette aspiration experiments that both leukocytes<sup>50</sup> and endothelial cells<sup>86</sup> exhibit an immediate elastic deformation followed by a much slower viscous deformation during suction. Such a behavior can be explained by the viscoelastic stress growth.

The effects of the cytoplasmic and nuclear viscosities on cell deformation and adhesion are illustrated on Figs. 11(b,c) and 12. An increase in the cytoplasmic viscosity at fixed nucleus-to-cytoplasm viscosity ratio leads to the decreased elongation of the cell. However, cell deformation at the contact area is observed even if the cytoplasm is very viscous [Fig. 11(b)]. An increase in viscosity of the nucleus at fixed viscosity of the cytoplasm changes the tear-drop shape of an adherent cell to a pear-like shape [Fig. 12(a)]. If the nuclear viscosity is much more than the cytoplasmic viscosity, the cell appears, from the top view, as a spherical body with a small extension at the contact area [Fig. 12(b)]. The microvillus contact time decreases with increasing the cytoplasmic or nuclear viscosity, i.e., with decreasing the cell deformability [Figs. 11(c) and 12(c)]. The less the microvillus contact time, the faster the cell can move. Therefore, if the cell rolls along the endothelium, its rolling velocity should decrease with the cell deformability, as recently suggested<sup>25,26</sup>.

The compound viscous drop model of the leukocyte was suggested as “the rheological basis for describing the leukocyte dynamics”<sup>11,87</sup>. Our results put in doubt this conclusion. Although this model takes into account the cytoplasm and the nucleus, it is oversimplified because all its phases are Newtonian liquids. Although the presence of the nucleus can lead to the viscoelastic response of the leukocyte in micropipette aspiration experiments, the main source for cell viscoelasticity is the cell cytoskeleton<sup>44,45</sup>, especially during cell adhesion in

circulation, when the cell diameter is less than the vessel diameter. Our 3D simulations show that the compound viscous model cannot predict a transition to a tear-drop shape observed for rolling leukocytes *in vivo*. The elasticity of the cell cytoplasm plays a crucial role in cell deformation under physiological conditions. The compound viscoelastic drop model discussed here takes into account both the presence of mechanically-different regions of the cell and the viscoelasticity of these regions.

Our numerical code can be used in the situations when the initial shape of the leukocyte is not spherical. Figure 13 shows the side and top views of the adherent monocyte (at different instants), which initial shape is obtained by cutting the bottom part of the sphere  $(x - x_c)^2 + (y - y_c)^2 + (z - z_c - z_{contact})^2 = a^2$  by the plane  $z = l_{mv} + l_{b0}$ . The coordinates of the sphere are  $x_c = 10 \mu\text{m}$ ,  $y_c = 25 \mu\text{m}$ , and  $z_c = a + l_{mv} + l_{b0}$ . In this case, the initial contact region of the monocyte is circular with radius  $R_{contact} = \sqrt{a^2 - (a - z_{contact})^2}$ . The formation of the finite contact region before rolling can occur due to normal forces acting on leukocytes in blood flow<sup>88</sup>. In the simulation,  $z_{contact} = 0.39 \mu\text{m}$  and there are 252 microvilli (distributed uniformly) with length  $l_{mv} = 0.38 \mu\text{m}$ . Hence,  $R_{contact} \approx 2.22 \mu\text{m}$ . 10 out of 252 microvilli are located in this region. Their nondimensional coordinates are given in Fig. 14(a). The rheological parameters of the viscoelastic cell shown in Fig. 13 are the same as in the previous case. However, its receptor-ligand interaction is characterized by low reverse reaction rate:  $k_{r0} = 0.1 \text{ s}^{-1}$ . As seen in this figure, the cell is detached from the plate by leaving two fragments of the cell membrane on the plate. We think that this happens due to the increased lifetime of bonds, i.e., if the bonds live in a stressed state for a sufficiently long time and the wall shear rate is sufficiently high, the cell membrane will be extended and disrupted. It is necessary to say that membrane rupture is observed *in vitro* during cell detachment under high shear<sup>89,90</sup>. Indeed, in the viscoelastic case, only one microvillus

(located near the trailing edge of the monocyte) is detached while other bonds are able to resist the drag force [Fig. 14(b)] for 1 ms and more. The critical length of the microvillus-bond spring is about  $1.04(l_{mv} + l_{b0})$  for the given set of kinetic parameters. Figure 14(b) also shows that the peripheral microvilli (denoted as No. 3 and 5) are responsible for the formation of cell debris. These microvilli lie a short distance from the trailing edge of the contact region (but not in the proximity of this edge as the detached microvillus), i.e, they are more extended and exert higher pulling force on the cell membrane than other ahead-positioned microvilli. The microvillus-bond spring length  $l_s$  of these two microvilli depends nonlinearly on time: it increases, reaches the maximum and then decreases [dashed line in Fig. 14(b)]. The membrane breakup seems to occur when the length reaches the maximum. Other microvilli are characterized by a monotonical time dependence of the microvillus-bond spring length. Note that the microvilli (and hence receptor-ligand bonds) are not equally stressed. The dependence of the spring length on the distance of the microvillus from the leading edge of the contact region  $d_{contact}$  can be represented by a polynomial curve as illustrated in Fig. 14(c).

An increase in the reverse reaction rate leads to decreasing the bond lifetime. We expect that a probability of membrane rupture is small in the case of short-lived bonds. Indeed, if the reverse reaction rate increases to  $1000 \text{ s}^{-1}$ , the cell is detached without the formation of cell debris (Fig. 15). The microvilli, which are responsible for membrane rupture in the case of low reverse reaction rate, reach the critical spring length  $1.03(l_{mv} + l_{b0})$  and separates from the plate due to bond dissociation before the membrane can be ruptured (Fig. 16).

### C. Monocyte adhesion: low wall shear rate

In all the discussed simulations, the monocyte is detached from the plate. This happens due to high WSR ( $\dot{\gamma}_w = 4000 \text{ s}^{-1}$  in those simulations). Meanwhile, the WSR is below  $800 \text{ s}^{-1}$  in postcapillary venules<sup>25,73</sup>, where leukocyte rolling is observed. We expect that leukocyte rolling can be captured by the numerical simulation at a smaller value of  $\dot{\gamma}_w$ . Indeed, if  $\tau_w = 0.4 \text{ Pa}$  and  $\dot{\gamma}_w = 400 \text{ s}^{-1}$ , monocyte rolling is observed (Fig. 17). In this simulation, we assume that the monocyte is a Newtonian cell which cytoplasm and nucleus have viscosities  $\mu_{cp}^s = 0.1 \text{ Pa}\cdot\text{s}$  and  $\mu_n^s = 1.0 \text{ Pa}\cdot\text{s}$ . The initial profile of the cell body is spherical and centered at  $(10 \mu\text{m}, 25 \mu\text{m}, 7.0 \mu\text{m})$ . The majority of 1236 microvilli of length  $0.49 \mu\text{m}$  are concentrated on the circle  $(x - x_c)^2 + (z - z_c)^2 = a^2$ . The reverse reaction rate constant  $k_{r0} = 1000 \text{ s}^{-1}$ . Figure 17 shows a 2-D slice of the cell (cross-section in the  $xz$ -plane at  $y = 25 \mu\text{m}$ ) together with the microvillus-bond springs (dashed lines) at different instants. Each closed circle denotes a linked microvillus. Each open circle signifies a microvillus detached from the plate. Seven microvilli are involved in cell adhesion for 1 ms. The old linked microvilli are come off after the next microvilli are attached to the plate. The new linked microvilli are always on the right (from the leading part of the cell) of the old linked microvilli. Hence, the monocyte rolls along the plate through the receptor-ligand interaction. The rolling velocity of this cell is about  $0.55 \mu\text{m}/\text{ms}$ . This value is significantly higher than in the experiments<sup>25</sup> because of high forward and reverse reaction rates in the simulation. Nevertheless, this velocity is smaller than the hydrodynamic velocity of the cell (the cell velocity in the case when receptor-ligand bonds are not formed). Based on Eq. (44), where  $z = z_c = 7.0 \mu\text{m}$ , the hydrodynamic velocity  $U_c$  is about  $2.2956 \mu\text{m}/\text{ms}$  for this cell.

The hydrodynamic velocity can also be calculated from the formula

$$U_c \approx z_c \dot{\gamma}_w \left[ 1 - \frac{5}{16} \left( \frac{a}{z_c} \right)^3 \right],$$

based on the lubrication-theory approximation for shear-induced motion of a solid sphere<sup>91</sup>.

This formula gives 2.099  $\mu\text{m}/\text{ms}$ .

The high value of the rolling velocity can also be attributed to the assumption that the cell is Newtonian used in the simulation. Even if the cell is characterized by small elasticity  $\lambda_1 = 0.01$  s, it is more deformed (Fig. 18) and rolls much slower than the Newtonian cell [Fig. 19(a)]. As pointed out by Olivier and Truskey<sup>92</sup>, the torque is very sensitive to the cell shape: it is diminished if the cell deviates from a spherical shape. Figure 19(b) shows that the bond lifetime increases by a factor of 6 due to increased deformability of the viscoelastic cell as recently suggested<sup>26</sup>.

## V. CONCLUSION

In this paper, we have studied numerically the effects of leukocyte deformability and viscoelasticity on leukocyte adhesion to a lower plate in a parallel-plate flow chamber. The study is done by using our own three-dimensional code in which the leukocyte with its surface folds (microvilli) is modeled as a compound viscoelastic drop with elastic rods distributed uniformly or nonuniformly over the leukocyte membrane. The leukocyte membrane is assumed to possess a cortical tension similar to a surface tension at fluid-fluid interface<sup>30</sup>. The spring-peeling kinetic model<sup>15</sup> modified to include the effects of microvillus extension and receptor extraction is used to describe adhesion of the leukocyte to the plate. The Giesekus constitutive equation is implemented in the code to capture the leukocyte viscoelasticity.

The numerical simulations have shown that if the leukocyte bulk elasticity is negligible,

i.e., if its cytoskeleton is weakened, the leukocyte membrane is elongated and disrupted in a manner similar to the formation and breakup of tethers from leukocyte microvilli observed *in vitro*<sup>28,83</sup>. This is consistent with the hypothesis that the formation of long tethers is associated with the local cytoskeleton failure where the cell membrane separates from the underlying actin cytoskeleton<sup>85</sup>. For the viscoelastic case, a transition from a spherical shape to a tear-drop shape typical for rolling leukocytes *in vivo*<sup>18</sup> is observed. The deformation to the tear-drop shape is explained by the positive first normal stress difference for the viscoelastic cell. The simulations show the microvillus contact time decreases with increasing the cell viscosity, i.e., with decreasing the cell deformability. This result lends support to the view that the cell rolling velocity decreases if the cell becomes more deformable<sup>25,26</sup>. We have also analyzed the effect of bond lifetime on leukocyte adhesion: if the receptor-ligand bonds live in a stressed state for a sufficiently long time, the leukocyte membrane can be extended and disrupted under high shear. In the case of finite contact area, peripheral microvilli are responsible for membrane rupture.

According to numerical simulations, leukocyte rolling along the plate is possible only if the wall shear rate is sufficiently low. Otherwise, the cell is detached from the plate. The leukocyte rolls slowly if its bulk elasticity is taken into account. This is most likely due to the increased deformability of the viscoelastic cell and, as a result, the decreased torque acting on this cell<sup>92</sup>.

Our next concerns will be the implementation of microvillus viscoelasticity and the two-receptor-mediated adhesion (selectin + integrin) into the code to model the viscous response of the microvillus during tether pulling<sup>28,84</sup> and the deceleration and subsequent firm adhesion of the rolling leukocyte<sup>4</sup>, respectively.

## **Acknowledgments**

This work is supported by National Institutes of Health under Grant No. HL-57446 and National Computational Science Alliance under Grant No. BCS040003N, and utilized the NCSA IBM p690. The authors thank Robert M. Hochmuth, Klaus Ley, Michael B. Lawrence, Ali Nadim, and Michael Renardy for stimulating and helpful discussions. The authors greatly acknowledge Robert M. Hochmuth, Klaus Ley, Scott L. Diamond, and David W. Schmidtke for providing images of leukocytes.

- 
- <sup>1</sup> J. Kuby, *Immunology, 2nd ed.* (W. H. Freeman and Company, New York, 1994).
- <sup>2</sup> B. Alberts, A. Johnson, J. Lewis, M. Raff, K. Roberts, and P. Walter, *Molecular Biology of the Cell, 4th ed.* (Garland, New York, 2002).
- <sup>3</sup> E. C. Butcher, “Leukocyte-endothelial cell recognition: three (or more) steps to specificity and diversity,” *Cell* **67**, 1033–1036 (1991).
- <sup>4</sup> K. Ley, “Molecular mechanisms of leukocyte recruitment in the inflammatory process,” *Cardiovasc. Res.* **32**, 733–742 (1996).
- <sup>5</sup> J. J. Campbell, J. Hedrick, A. Zlotnik, M. A. Siani, D. A. Thompson, and E. C. Butcher, “Chemokines and the arrest of lymphocytes rolling under flow conditions,” *Science* **279**, 381–384 (1998).
- <sup>6</sup> J. E. Blanks, T. Moll, R. Eytner, and D. Vestweber, “Stimulation of P-selectin glycoprotein ligand-1 on mouse neutrophils activates  $\beta_2$ -integrin mediated cell attachment to ICAM-1,” *Eur. J. Immunol.* **28**, 433–443 (1998).
- <sup>7</sup> P. Tandon and S. L. Diamond, “Hydrodynamic effects and receptor interactions of platelets and their aggregates in linear shear flow,” *Biophys. J.* **73**, 2819–2835 (1997).
- <sup>8</sup> Y. Zhao, S. Chien, and S. Weinbaum, “Dynamic contact forces on leukocyte microvilli and their penetration of the endothelial glycocalyx,” *Biophys. J.* **80**, 1124–1140 (2001).
- <sup>9</sup> D. A. Hammer and D. A. Lauffenburger, “A dynamical model for receptor-mediated cell adhesion to surfaces,” *Biophys. J.* **52**, 475–487 (1987).

- <sup>10</sup> D. A. Hammer and S. M. Apte, “Simulation of cell rolling and adhesion on surfaces in shear flow: general results and analysis of selectin-mediated neutrophil adhesion,” *Biophys. J.* **63**, 35–57 (1992).
- <sup>11</sup> N. A. N’Dri, W. Shyy, and R. Tran-Son-Tay, “Computational modeling of cell adhesion and movement using a continuum-kinetics approach,” *Biophys. J.* **85**, 2273–2286 (2003).
- <sup>12</sup> C. Dong, J. Cao, E. J. Struble, and H. H. Lipowsky, “Mechanics of leukocyte deformation and adhesion to endothelium in shear flow,” *Ann. Biomed. Eng.* **27**, 298–312 (1999).
- <sup>13</sup> M. R. King and D. A. Hammer, “Multiparticle adhesive dynamics: Hydrodynamic recruitment of rolling leukocytes,” *Proc. Nat. Acad. Sci.* **98**, 14919–14924 (2001).
- <sup>14</sup> G. I. Bell, “Models for the specific adhesion of cells to cells,” *Science* **200**, 618–627 (1978).
- <sup>15</sup> M. Dembo, D. C. Torney, K. Saxman, and D. A. Hammer, “The reaction-limited kinetics of membrane-to-surface adhesion and detachment,” *Proc. R. Soc. London* **234**, 55–83 (1988).
- <sup>16</sup> K.-C. Chang, D. F. J. Tees, and D. A. Hammer, “The state diagram for cell adhesion under flow: Leukocyte rolling and firm adhesion,” *Proc. Nat. Acad. Sci.* **97**, 11262–11267 (2000).
- <sup>17</sup> J. C. Firell and H. H. Lipowsky, “Leukocyte margination and deformation in mesenteric venules of rat,” *Am. J. Physiol.* **256**, H1667–H1674 (1989).
- <sup>18</sup> E. R. Damiano, J. Westheider, A. Tozeren, and K. Ley, “Variation in the velocity, deformation, and adhesion energy density of leukocytes rolling within venules,” *Circ. Res.* **79**, 1122–1130 (1996).
- <sup>19</sup> R. M. Hochmuth, H. P. Ting-Beall, B. B. Beaty, D. Needham, and R. Tran-Son-Tay, “Viscosity

- of passive human neutrophils undergoing small deformations,” *Biophys. J.* **64**, 1596–1601 (1993).
- <sup>20</sup> R. Tran-Son-Tay, D. Needham, A. Yeung, and R. M. Hochmuth, “Time-dependent recovery of passive neutrophils after large deformation,” *Biophys. J.* **60**, 856–866 (1991).
- <sup>21</sup> M. B. Lawrence and T. A. Springer, “Leukocytes roll on a selectin at physiologic flow rates: Distinction from and prerequisite for adhesion through integrins,” *Cell* **65**, 859–873 (1991).
- <sup>22</sup> J. Cao, B. Donell, D. R. Deaver, M. B. Lawrence, and C. Dong, “*In vitro* side-view imaging technique and analysis of human T-leukemic cell adhesion to ICAM-1 in shear flow,” *Microvasc. Res.* **55**, 124–137 (1998).
- <sup>23</sup> R. Alon, S. Chen, R. Fuhlbridge, K. D. Puri, and T. A. Springer, “The kinetics and shear threshold of transient and rolling interactions of L-selectin with its ligand on leukocytes,” *Proc. Natl. Acad. Sci.* **95**, 11631–11636 (1998).
- <sup>24</sup> S. Chen and T. A. Springer, “An automatic braking system that stabilizes leukocyte rolling by an increase in selectin bond number with shear,” *J. Cell Biol.* **144**, 185–200 (1999).
- <sup>25</sup> M. L. Smith, M. J. Smith, M. B. Lawrence, and K. Ley, “Viscosity-independent velocity of neutrophils rolling on P-selectin *in vitro* or *in vivo*,” *Microcirculation* **9**, 523–536 (2002).
- <sup>26</sup> K. D. Rinker, V. Prabhakar, and G. A. Truskey, “Effect of contact time and force on monocyte adhesion to vascular endothelium,” *Biophys. J.* **80**, 1722–1732 (2001).
- <sup>27</sup> C. Dong and X. X. Lei, “Biomechanics of cell rolling: shear flow, cell-surface adhesion, and cell deformability,” *J. Biomech.* **33**, 35–43 (2000).

- <sup>28</sup> J.-Y. Shao, H. P. Ting-Beall, and R. M. Hochmuth, “Static and dynamic lengths of neutrophil microvilli,” *Proc. Natl. Acad. Sci.* **95**, 6797–6802 (1998).
- <sup>29</sup> U. H. von Andrian, S. R. Hasslen, S. Erlandsen, and E. C. Butcher, “A central role for microvillous receptor presentation in leukocyte adhesion under flow,” *Cell* **82**, 989–999 (1995).
- <sup>30</sup> D. V. Zhelev, D. Needham, and R. M. Hochmuth, “Role of the membrane cortex in neutrophil deformation in small pipets,” *Biophys. J.* **67**, 696–705 (1994).
- <sup>31</sup> J.-Y. Shao and R. M. Hochmuth, “Micropipette suction for measuring piconewton forces of adhesion and tether formation from neutrophil membranes,” *Biophys. J.* **71**, 2892–2901 (1996).
- <sup>32</sup> F. M. Pavalko and S. M. LaRoche, “Activation of human neutrophils induces an interaction between the integrin  $\beta_2$ -subunit (CD18) and the actin binding protein  $\alpha$ -actinin,” *J. Immunol.* **151**, 3795–3807 (1993).
- <sup>33</sup> F. M. Pavalko, D. M. Walker, L. Graham, M. Goheen, C. M. Doerschuk, and G. S. Kansas, “The cytoplasmic domain of L-selectin interacts with cytoskeletal proteins via  $\alpha$ -actinin: receptor positioning in microvilli does not require interaction with  $\alpha$ -actinin,” *J. Cell Biol.* **129**, 1155–1164 (1995).
- <sup>34</sup> E. B. Finger, K. D. Puri, R. Alon, M. B. Lawrence, U. H. von Andrian, and T. A. Springer, “Adhesion through L-selectin requires a threshold hydrodynamic shear,” *Nature* **379**, 266–269 (1996).
- <sup>35</sup> M. B. Lawrence, G. S. Kansas, E. J. Kunkel, and K. Ley, “Threshold levels of fluid shear

- promote leukocyte adhesion through selectins (CD62L,P,E),” *J. Cell Biol.* **136**, 717–727 (1997).
- <sup>36</sup> K. Konstantopoulos, W. D. Hanley, and D. Wirtz, “Receptor-ligand binding: ‘catch’ bonds finally caught,” *Current Biology* **13**, R611–R613 (2003).
- <sup>37</sup> B. T. Marshall, M. Long, J. W. Piper, T. Yago, R. P. McEver, and C. Zhu, “Direct observation of catch bonds involving cell-adhesion molecules,” *Nature* **423**, 190–193 (2003).
- <sup>38</sup> D. C. Anderson, “The role of  $\beta_2$ -integrins and intercellular adhesion molecule type 1 in inflammation,” in *Physiology and Pathophysiology of Leukocyte Adhesion*, edited by D. N. Granger and G. W. Schmid-Schönbein (Oxford University Press, New York, 1994), pp. 3–42.
- <sup>39</sup> M. Forrest and J. C. Paulson, “Selectin family of adhesion molecules,” in *Physiology and Pathophysiology of Leukocyte Adhesion*, edited by D. N. Granger and G. W. Schmid-Schönbein (Oxford University Press, New York, 1994), pp. 43–80.
- <sup>40</sup> J.-Y. Shao and R. M. Hochmuth, “Mechanical anchoring strength of L-selectin,  $\beta_2$  integrins, and CD45 to neutrophil cytoskeleton and membrane,” *Biophys. J.* **77**, 587–596 (1999).
- <sup>41</sup> A. Hafezi-Moghadam and K. Ley, “Relevance of L-selectin shedding for leukocyte rolling in vivo,” *J. Exp. Med.* **189**, 939–947 (1999).
- <sup>42</sup> B. P. Chan, W. M. Reichert, and G. A. Truskey, “Effect of streptavidin-biotin on endothelial vasoregulation and leukocyte adhesion,” *Biomaterials*, accepted (2003).
- <sup>43</sup> Y. Tseng, T. P. Kole, S.-H. J. Lee, and D. Wirtz, “Local dynamics and viscoelastic properties of cell biological systems,” *Curr. Op. Coll. Interface Sci.* **7**, 210–217 (2002).

- <sup>44</sup> B. Fabry, G. N. Maksym, J. P. Butler, M. Glogauer, D. Navajas, and J. J. Fredberg, “Scaling the microrheology of living cells,” *Phys. Rev. Lett.* **87**, (148102) (2001).
- <sup>45</sup> A. W. C. Lau, B. D. Hoffman, A. Davies, J. C. Crocker, and T. C. Lubensky, “Microrheology, stress fluctuations and active behavior of living cells,” *Phys. Rev. Lett.* **91**, (198101) (2003).
- <sup>46</sup> G. W. Schmid-Schönbein, “Rheology of leukocytes,” in *Handbook of Bioengineering*, edited by R. Skalak and S. Chien (McGraw-Hill, New York, 1986), pp. 13.1–13.25.
- <sup>47</sup> C. Dong, R. Skalak, K.-L. P. Sung, G. W. Schmid-Schönbein, and S. Chien, “Passive deformation analysis of human leukocytes,” *J. Biomech. Eng.* **110**, 27–36 (1988).
- <sup>48</sup> M. A. Tsai, R. S. Frank, and R. E. Waugh, “Passive mechanical behavior of human neutrophils: power-law fluid,” *Biophys. J.* **65**, 2078–2088 (1993).
- <sup>49</sup> J. L. Drury and M. Dembo, “Aspiration of human neutrophils: effect of shear thinning and cortical dissipation,” *Biophys. J.* **81**, 3166–3177 (2001).
- <sup>50</sup> R. M. Hochmuth, “Micropipette aspiration of living cells,” *J. Biomech.* **33**, 15–22 (2000).
- <sup>51</sup> E. Evans and B. Kukan, “Passive material behavior of granulocytes based on large deformation and recovery after deformation tests,” *Blood* **64**, 1028–1035 (1984).
- <sup>52</sup> R. E. Waugh and M. A. Tsai, “Shear rate-dependence of leukocyte cytoplasmic viscosity,” in *Cell Mechanics and Cellular Engineering*, edited by V. C. Mow, R. Tran-Son-Tay, F. Guilak, and R. N. Hochmuth (Springer-Verlag, New York, 1994), pp. 33–45.
- <sup>53</sup> R. B. Bird, R. C. Armstrong, and O. Hassager, *Dynamics of Polymeric Liquids, Vol. 1: Fluid Mechanics* (Wiley, New York, 1987).

- <sup>54</sup> H. Giesekus, “A simple constitutive equation for polymer fluids based on the concept of deformation-dependent tensorial mobility,” *J. Non-Newtonian Fluid Mech.* **11**, 69–109 (1982).
- <sup>55</sup> H. Giesekus, “Stressing behaviour in simple shear flow as predicted by a new constitutive model for polymer fluids,” *J. Non-Newtonian Fluid Mech.* **12**, 367–374 (1983).
- <sup>56</sup> H. Giesekus, “Constitutive equations for polymer fluids based on the concept of configuration-dependent molecular mobility: a generalized mean-configuration model,” *J. Non-Newtonian Fluid Mech.* **17**, 349–372 (1985).
- <sup>57</sup> D. Gueyffier, J. Li, A. Nadim, R. Scardovelli, and S. Zaleski, “Volume-of-fluid interface tracking and smoothed surface stress methods for three-dimensional flows,” *J. Comp. Phys.* **152**, 423–456 (1999).
- <sup>58</sup> R. Scardovelli and S. Zaleski, “Direct numerical simulation of free surface and interfacial flow,” *Ann. Rev. Fluid Mech.* **31**, 567–604 (1999).
- <sup>59</sup> C. W. Hirt and B. D. Nichols, “Volume of fluid (VOF) method for the dynamics of free boundaries,” *J. Comp. Phys.* **39**, 201–225 (1981).
- <sup>60</sup> J. Li, “Calcul d’interface affine par morceaux (piecewise linear interface calculation),” *C. R. Acad. Sci. Paris t. 320 série IIb*, 391–396 (1995).
- <sup>61</sup> J. U. Brackbill, D. B. Kothe, and C. Zemach, “A continuum method for modeling surface tension,” *J. Comp. Phys.* **100**, 335–354 (1992).
- <sup>62</sup> I. Aleinov and E. G. Puckett, “Computing surface tension with high-order kernels,” in *Proceedings of the 6th International Symposium on Computational Fluid Dynamics*, edited by K. Oshima (Lake Tahoe, Nevada, 1995), pp. 13–18.

- <sup>63</sup> A. J. Chorin, “A numerical method for solving incompressible viscous flow problems,” *J. Comp. Phys.* **2**, 12–26 (1967).
- <sup>64</sup> P. J. Roache, *Fundamentals of Computational Fluid Dynamics* (Hermosa, Albuquerque, 1998).
- <sup>65</sup> J. Li, Y. Renardy, and M. Renardy, “Numerical simulation of breakup of a viscous drop in simple shear flow through a volume-of-fluid method,” *Phys. Fluids* **12**, 269–282 (2000).
- <sup>66</sup> J. Li, Y. Renardy, and M. Renardy, “A numerical study of periodic disturbances on two-layer couette flow,” *Phys. Fluids* **10**, 3056–3071 (1998).
- <sup>67</sup> Y. Zang, R. L. Street, and J. R. Koseff, “A non-staggered grid, fractional step method for time-dependent incompressible Navier-Stokes equations in curvilinear coordinates,” *J. Comp. Phys.* **114**, 18–33 (1994).
- <sup>68</sup> B. Lafaurie, C. Nardone, R. Scardovelli, S. Zaleski, and G. Zanetti, “Modelling merging and fragmentation in multiphase flows with SURFER,” *J. Comp. Phys.* **113**, 134–147 (1994).
- <sup>69</sup> M. J. Crochet, A. R. Davies, and K. Walters, *Numerical Simulation of Non-Newtonian Flow* (Elsevier, New York, 1984).
- <sup>70</sup> J. Fritz, A. G. Katopodis, F. Kolbinger, and D. Anselmetti, “Force-mediated kinetics of single P-selectin / ligand complexes observed by atomic force microscopy,” *Proc. Natl. Acad. Sci.* **95**, 12283–12288 (1998).
- <sup>71</sup> T. A. Springer, “Adhesion receptors of the immune system,” *Nature* **346**, 425–434 (1990).
- <sup>72</sup> H. P. Ting-Beall, D. Needham, and R. M. Hochmuth, “Volume and osmotic properties of human

- neutrophils,” *Blood* **81**, 2774–2780 (1993).
- <sup>73</sup> H. H. Lipowsky, “Mechanics of blood flow in the microcirculation,” in *Handbook of Bioengineering*, edited by R. Skalak and S. Chien (McGraw-Hill, New York, 1986), pp. 18.1–18.25.
- <sup>74</sup> E. M. Renkin, “Microcirculation and exchange,” in *Textbook of Physiology*, edited by H. D. Patton, A. F. Fuchs, B. Hille, A. M. Scher, and R. Steiner (W. B. Saunders Company, Philadelphia, 1989), pp. 860–886.
- <sup>75</sup> S. E. Chesla, P. Selvaraj, and C. Zhu, “Measuring two-dimensional receptor-ligand binding kinetics by micropipette,” *Biophys. J.* **75**, 1553–1572 (1998).
- <sup>76</sup> E. Y. H. Park, M. J. Smith, E. S. Stropp, K. R. Snapp, J. A. DiVetro, W. F. Walker, D. W. Schmidtke, S. L. Diamond, and M. B. Lawrence, “Comparison of PSGL-1 microbead and neutrophil rolling: microvillus elongation stabilizes P-selectin bond clusters,” *Biophys. J.* **82**, 1835–1847 (2002).
- <sup>77</sup> G. Kaplanski, C. Farnarier, O. Tissot, A. Pierres, A. Benoliel, M. C. Alessi, S. Kaplanski, and P. Bongrand, “Granulocyte-endothelium initial adhesion: analysis of transient binding events mediated by E-selectin in a laminar shear flow,” *Biophys. J.* **64**, 1922–1933 (1993).
- <sup>78</sup> F. Geissmann, S. Jung, and D. R. Littman, “Blood monocytes consist of two principal subsets with distinct migratory properties,” *Immunity* **19**, 71–82 (2003).
- <sup>79</sup> R. Ross, “Mechanisms of disease: atherosclerosis - an inflammatory disease,” *N. Engl. J. Med.* **340**, 115–126 (1999).
- <sup>80</sup> A. J. Lusis, “Atherosclerosis,” *Nature* **407**, 233–241 (2000).

- <sup>81</sup> T. W. Secomb, R. Hsu, and A. R. Pries, “Motion of red blood cells in a capillary with an endothelial surface layer: effect of flow velocity,” *Am. J. Physiol.* **281**, H629–H636 (2001).
- <sup>82</sup> A. Nadim and H. A. Stone, “The motion of small particles and droplets in quadratic flows,” *Stud. Appl. Math.* **85**, 53–73 (1991).
- <sup>83</sup> D. W. Schmidtke and S. L. Diamond, “Direct observation of membrane tethers formed during neutrophil attachment to platelets or P-selectin under physiological flow,” *J. Cell Biol.* **149**, 719–729 (2000).
- <sup>84</sup> R. M. Hochmuth and W. D. Marcus, “Membrane tethers formed from blood cells with available area and determination of their adhesion energy,” *Biophys. J.* **82**, 2964–2969 (2002).
- <sup>85</sup> W. D. Marcus and R. M. Hochmuth, “Experimental studies of membrane tethers formed from human neutrophils,” *Ann. Biomed. Eng.* **30**, 1273–1280 (2002).
- <sup>86</sup> M. Sato, N. Ohshima, and R. M. Nerem, “Viscoelastic properties of cultured porcine aortic endothelial cells exposed to shear stress,” *J. Biomech.* **29**, 461–467 (1996).
- <sup>87</sup> H.-C. Kan, W. Shyy, H. S. Udaykumar, P. Vigneron, and R. Tran-Son-Tay, “Effects of nucleus on leukocyte recovery,” *Ann. Biomed. Eng.* **27**, 648–655 (1999).
- <sup>88</sup> C. Migliorini, Y.-H. Qian, E. B. Brown, R. K. Jain, and L. L. Munn, “Red blood cells augment leukocyte rolling in a virtual blood vessel,” *Biophys. J.* **83**, 1834–1841 (2002).
- <sup>89</sup> G. A. Truskey and T. L. Proulx, “Relationship between 3T3 cell spreading and the strength of adhesion on glass and silane surfaces,” *Biomaterials* **14**, 243–254 (1993).
- <sup>90</sup> A. S. Goldstein and P. A. DiMilla, “Examination of membrane rupture as a mechanism for

mammalian cell detachment from fibronectin-coated biomaterials,” *J. Biomed. Mater. Res.* **67**, 658–666 (2003).

<sup>91</sup> A. J. Goldman, R. G. Cox, and H. Brenner, “Slow viscous motion of a sphere parallel to a plane wall - II. Couette flow,” *Chem Eng. Sci.* **22**, 653–660 (1967).

<sup>92</sup> L. A. Olivier and G. A. Truskey, “A numerical analysis of forces exerted by laminar flow on spreading cells in a parallel plate flow chamber assay,” *Biotechnol. Bioeng.* **42**, 963–973 (1993).

## FIGURE CAPTIONS

**Fig. 1.** Scanning electron micrograph of a human neutrophil. The image was provided by Dr. Robert M. Hochmuth (Department of Mechanical Engineering and Materials Science, Duke University).

**Fig. 2.** Schematic drawing of the leukocyte model used in the numerical simulations. The leukocyte is modeled as a 3D compound viscoelastic drop which shell and core phases represent the leukocyte cytoplasm and nucleus. The leukocyte membrane is assumed to be very thin and to possess a cortical tension. The membrane ruffles (microvilli) are modeled as elastic rods with receptors on their tips. Bonds between receptors and ligands are Hookean springs.

**Fig. 3.** Schematic drawing of the flow domain. The leukocyte is suspended in a low-viscosity liquid (extracellular fluid) between the fixed upper and lower plates. The shear flow is created by the pressure drop between the left and right boundaries  $P_i - P_o$ . The  $x$ -axis coincides with the flow direction. The  $y$  and  $z$  axes are perpendicular to the flow. The  $d_x$ ,  $d_y$ , and  $d_z$  are the dimensions of the computational domain.

**Fig. 4.** Marker-And-Cell grid cell. The  $\Delta x$ ,  $\Delta y$ , and  $\Delta z$  are the grid cell sizes (spatial steps in the  $x$ ,  $y$  and  $z$  directions). The grid cell indexes are denoted by  $i$ ,  $j$ , and  $k$ .

**Fig. 5.** Computed neutrophil shape and velocity field at different instances: cross-section in the  $xz$ -plane at  $y = 20 \mu\text{m}$ . The neutrophil moves in the central flow stream. It is modeled as a compound Newtonian cell of radius  $a = 4 \mu\text{m}$ , which is characterized by the cytoplasmic and nuclear viscosities  $\mu_{cp}^s = 0.001 \text{ Pa}\cdot\text{s} = 1 \text{ cP}$  and  $\mu_n^s = 0.1 \text{ Pa}\cdot\text{s} = 1 \text{ P}$ . The wall shear stress and wall shear rate  $\tau_w = 4 \text{ Pa}$  and  $\dot{\gamma}_w = 4000 \text{ s}^{-1}$ . The

computational domain is  $40 \mu\text{m} \times 40 \mu\text{m} \times 16 \mu\text{m}$ . The number of grid cells is  $128 \times 128 \times 64$ . The leading edge of the neutrophil is elongated in the form of paraboloid and its trailing edge is flattened.

**Fig. 6.** Computed shape of the adherent neutrophil and velocity field at different instances: cross-section in the  $xz$ -plane at  $y = 20 \mu\text{m}$ . The neutrophil is a compound Newtonian cell which cytoplasmic and nuclear viscosities  $\mu_{cp}^s = 0.1 \text{ Pa}\cdot\text{s} = 1 \text{ P}$  and  $\mu_n^s = 1.0 \text{ Pa}\cdot\text{s} = 10 \text{ P}$ . Initially, the neutrophil center is located at  $(8 \mu\text{m}, 20 \mu\text{m}, 4.1 \mu\text{m})$ . 1089 microvilli of length  $l_{mv} = 0.09 \mu\text{m}$  are distributed nonuniformly (they are concentrated at the bottom of the cell). Adhesion parameters:  $\sigma_b = 5300 \text{ pN}/\mu\text{m}$ ,  $\sigma_{mv} = 340 \text{ pN}/\mu\text{m}$ ,  $\sigma_{tss} = 160 \text{ pN}/\mu\text{m}$ ,  $l_{b0} = 0.01 \mu\text{m}$ ,  $r_{mv} = 0.1 \mu\text{m}$ ,  $\gamma = 2.0625$ ,  $n_r = 5 \times 10^3 \mu\text{m}^{-2}$ ,  $n_l = 5 \times 10^4 \mu\text{m}^{-2}$ ,  $k_{f0} = 10 \mu\text{m}^2/\text{s}$ , and  $k_{r0} = 1 \text{ s}^{-1}$ . The adhesion part of the neutrophil membrane is stretched in the direction of the microvillus-bond spring force.

**Fig. 7.** Snapshots of monocyte shape (side view). The monocyte is a compound Newtonian drop of radius  $6.5 \mu\text{m}$ . Its cytoplasmic and nuclear viscosities  $\mu_{cp}^s = 0.1 \text{ Pa}\cdot\text{s} = 1 \text{ P}$  and  $\mu_n^s = 1.0 \text{ Pa}\cdot\text{s} = 10 \text{ P}$ . Initially, the monocyte is centered at  $(10 \mu\text{m}, 25 \mu\text{m}, 6.6 \mu\text{m})$ . 252 microvilli of length  $l_{mv} = 0.09 \mu\text{m}$  are distributed uniformly. Adhesion parameters:  $\sigma_b = 5300 \text{ pN}/\mu\text{m}$ ,  $\sigma_{mv} = 210 \text{ pN}/\mu\text{m}$ ,  $\sigma_{tss} = 100 \text{ pN}/\mu\text{m}$ ,  $l_{b0} = 0.01 \mu\text{m}$ ,  $r_{mv} = 0.1 \mu\text{m}$ ,  $\gamma = 3$ ,  $n_r = 1.5 \times 10^3 \mu\text{m}^{-2}$ ,  $n_l = 3 \times 10^3 \mu\text{m}^{-2}$ ,  $k_{f0} = 100 \mu\text{m}^2/\text{s}$ , and  $k_{r0} = 100 \text{ s}^{-1}$ . The computational domain is  $50 \mu\text{m} \times 50 \mu\text{m} \times 50 \mu\text{m}$ . The number of grid cells is  $64 \times 64 \times 128$ . The fast elongation and breakup of the monocyte membrane are observed.

**Fig. 8.** Comparison of (a) *in vitro* images and (b) computed shapes of the adherent leuko-

cyte. (a) Neutrophil on a P-selectin-coated surface of the parallel-plate flow chamber at a wall shear rate of  $150 \text{ s}^{-1}$ . A single tether is pulled and broken up. The images were provided by the Diamond Laboratory (Institute for Medicine and Engineering, University of Pennsylvania). (b) Top view of the cell shown in Fig. 7. The wall shear rate is  $4000 \text{ s}^{-1}$ .

**Fig. 9.** Snapshots of monocyte shape (side view). The monocyte is a compound viscoelastic drop. The solvent and polymer viscosities of the cytoplasm  $\mu_{cp}^s = 0.001 \text{ Pa}\cdot\text{s} = 1 \text{ cP}$  and  $\mu_{cp}^p = 3.528 \text{ Pa}\cdot\text{s} = 35.28 \text{ P}$ . The solvent and polymer viscosities of the nucleus  $\mu_n^s = 0.001 \text{ Pa}\cdot\text{s} = 1 \text{ cP}$  and  $\mu_n^p = 10 \text{ Pa}\cdot\text{s} = 100 \text{ P}$ . The cytoplasmic and nuclear relaxation times  $\lambda_{1cp} = 0.176 \text{ s}$  and  $\lambda_{1n} = 0.200 \text{ s}$ . The reverse reaction rate constant  $k_{r0} = 10 \text{ s}^{-1}$ . The remaining parameters are listed in Fig. 7. The cell is deformed to a tear-drop shape.

**Fig. 10.** Top view of the cell shown in Fig. 9. A small fragment of the cell membrane is left on the plate.

**Fig. 11.** (a) *In vivo* image of rolling neutrophils. A postcapillary venule of the rat mesentery. The rolling neutrophils are deformed to a tear-drop shape. The images were provided by Klaus Ley (Department of Biomedical Engineering, University of Virginia, unpublished). (b) Computed shapes of an adherent viscoelastic cell (side view) for different cytoplasmic viscosities at  $t = 0.8 \text{ ms}$ . The viscoelastic cell is deformed to a tear-drop shape for a wide range of polymer viscosities. (c) Microvillus contact time as a function of the cytoplasmic viscosity. In both (b) and (c), the nucleus-to-cytoplasm viscosity ratio is fixed ( $\mu_n/m\mu_{cp} \approx 2.8$ ). The remaining parameters are listed in Figs. 7 and 9.

**Fig. 12.** (a) Side and (b) top views of an adherent viscoelastic cell for different nuclear viscosities at  $t = 0.8$  ms. The cytoplasmic viscosity is fixed ( $\mu_{cp} = 3.529$  Pa·s = 35.29 P). The remaining parameters are listed in Figs. 7 and 9. The cell is deformed to a pear-like shape at large nucleus-to-cytoplasm viscosity ratios. (c) Microvillus contact time as a function of the nucleus-to-cytoplasm viscosity ratio.

**Fig. 13.** Side and top views of the adherent monocyte at different instants. The monocyte is viscoelastic but its initial shape is not spherical. The contact region is circular with radius of about  $2.2221 \mu\text{m}$ . 10 out of 252 microvilli are located in the contact region. The microvillus length is  $0.381625 \mu\text{m}$ . The reverse reaction rate constant is small:  $k_{r0} = 0.1 \text{ s}^{-1}$ . The remaining parameters are listed in Figs. 7 and 9. The monocyte is detached from the plate by leaving two fragments (debris) of the membrane.

**Fig. 14.** (a) Nondimensional coordinates of 10 microvilli in the contact region at  $t = 0$  ms for the cell shown in Fig. 13.  $P_0$  and  $R_{contact}$  are the leading edge and radius of the contact region. The characteristic length  $l_* = 50 \mu\text{m}$ . (b) Relative length of the microvillus-bond spring  $l_s/l_{s0}$  versus time for 10 linked microvilli. The unstressed length  $l_{s0} = l_{mv} + l_{b0}$ . The characteristic time  $t_* = 1.67$  ms. Two peripheral microvilli (No. 3 and 5) are responsible for the formation of cell debris. The spring length for these two microvilli goes through the maximum at which membrane rupture occurs. (c) Relative length of the microvillus-bond spring as a function of the nondimensional distance  $\bar{d}_{contact}$  from a microvillus to the leading edge of the contact region ( $P_0$ ) at  $t = 0.4t_*$  and  $t = 0.5t_*$ .

**Fig. 15.** Side and top views of the adherent monocyte at different instants. As compared to the cell shown in Fig. 13, the reverse reaction rate constant is large:  $k_{r0} = 1000$

$\text{s}^{-1}$ . The remaining parameters are the same. The monocyte is detached without the formation of cell debris.

**Fig. 16.** Relative length of the microvillus-bond spring  $l_s/l_{s0}$  versus time for microvilli No. 3 and 5 [cf. Fig. 14(a)]. The solid and dashed lines correspond to  $k_{r0} = 0.1$  and  $1000 \text{ s}^{-1}$ , respectively. In the case of high reverse reaction rate, these microvilli detach before the instant when the membrane can be ruptured.

**Fig. 17.** Bottom part of the monocyte and microvillus bond springs at low wall shear stress: cross-section in the  $xz$ -plane at  $y = 25 \mu\text{m}$ . The monocyte is modeled as a Newtonian cell. The cell cytoplasm and nucleus have viscosities  $\mu_{cp}^s = 0.1 \text{ Pa}\cdot\text{s} = 1 \text{ P}$  and  $\mu_n^s = 1.0 \text{ Pa}\cdot\text{s} = 10 \text{ P}$ . The wall shear stress and wall shear rate  $\tau_w = 0.4 \text{ Pa}$  and  $\dot{\gamma}_w = 400 \text{ s}^{-1}$ . 1236 microvilli of length  $0.49 \mu\text{m}$  are concentrated on the circle  $(x - x_c)^2 + (z - z_c)^2 = a^2$ , where the cell center coordinates  $(x_c, y_c, z_c) = (10 \mu\text{m}, 25 \mu\text{m}, 7.0 \mu\text{m})$ . The reverse reaction rate constant  $k_{r0} = 1000 \text{ s}^{-1}$ . The remaining adhesion parameters are listed in Fig. 7. Closed and open circles denote a linked and detached microvilli, respectively. Dashed lines are microvillus-bond springs. Cell rolling is observed. The cell undergoes negligible deformation.

**Fig. 18.** Snapshots of monocyte shape (side view) at low wall shear stress. The monocyte is modeled as a viscoelastic cell. The relaxation times of the cytoplasm and nucleus are equal:  $\lambda_{1cp} = \lambda_{1n} = 0.01 \text{ s}$ . The polymer viscosities of the cytoplasm and nucleus  $\mu_{cp}^p = 0.099 \text{ Pa}\cdot\text{s} = 0.99 \text{ P}$  and  $\mu_n^p = 0.999 \text{ Pa}\cdot\text{s} = 9.99 \text{ P}$ . The remaining parameters are listed in Figs. 7 and 17. The viscoelastic cell is more deformed and rotates slower than the Newtonian cell.

**Fig. 19.** (a) Nondimensional  $x$ -coordinate of the microvillus base versus time for the first

linked microvilli. Solid line is a Newtonian cell (Fig. 17). Dashed line is a viscoelastic cell (Fig. 18). The characteristic time and length  $t_* = 1.67$  ms and  $l_* = 50$   $\mu$ m. The displacement of the microvillus in flow direction is greater in the Newtonian case than in the viscoelastic case: the rolling velocity of the viscoelastic cell is smaller than that of the Newtonian cell. (b) Relative length of the microvillus-bond spring  $l_s/l_{s0}$  versus time for the second linked microvillus. The microvillus contact time increases significantly in the viscoelastic case as compared to the Newtonian case due to the increased deformability of the viscoelastic cell.

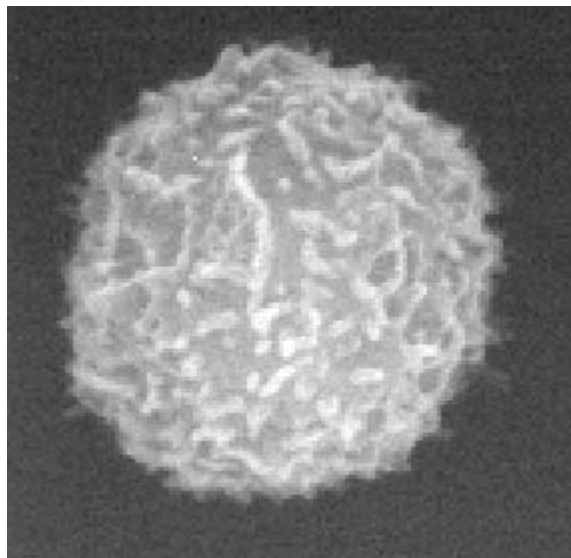


Fig. 1

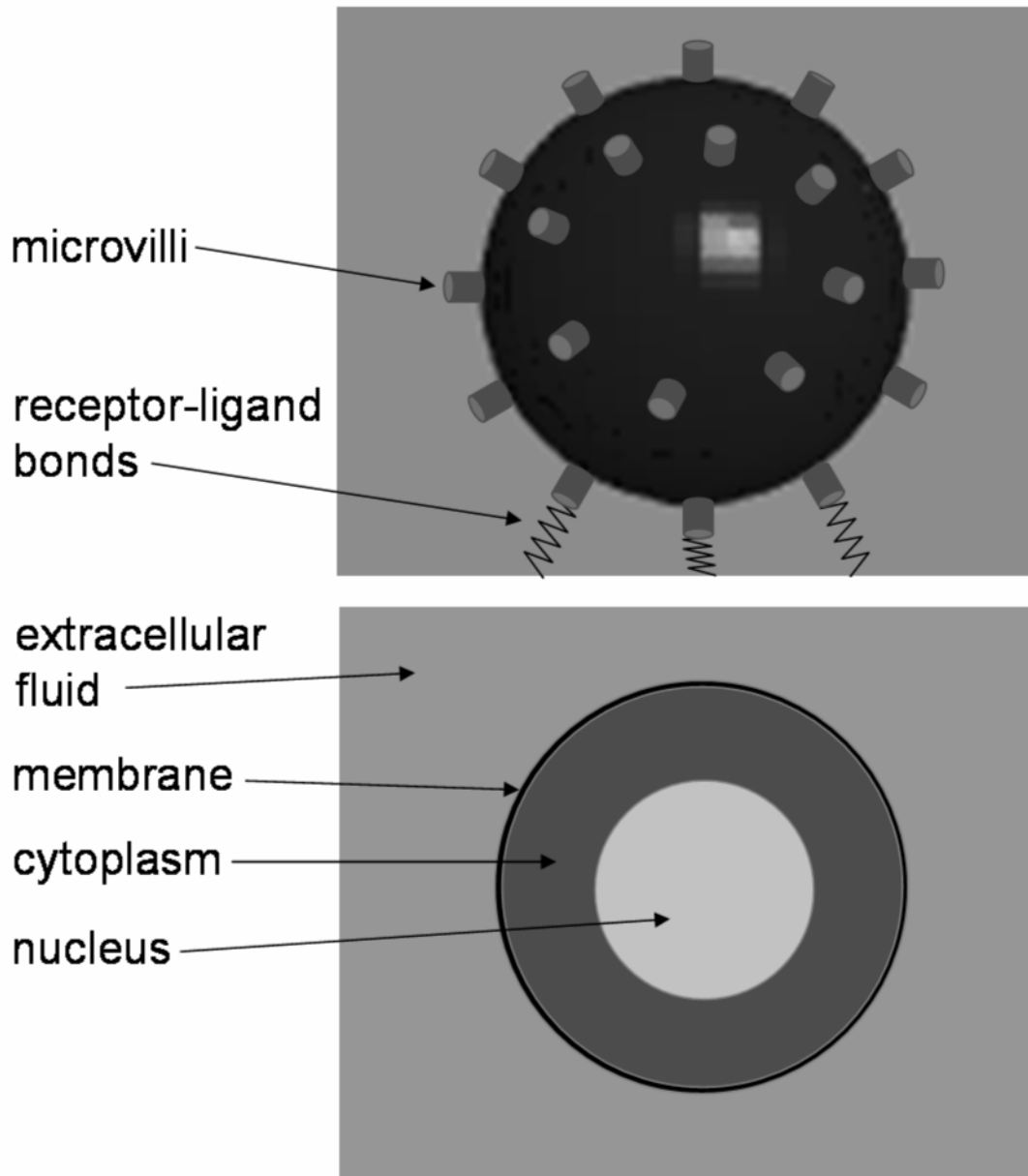


Fig. 2

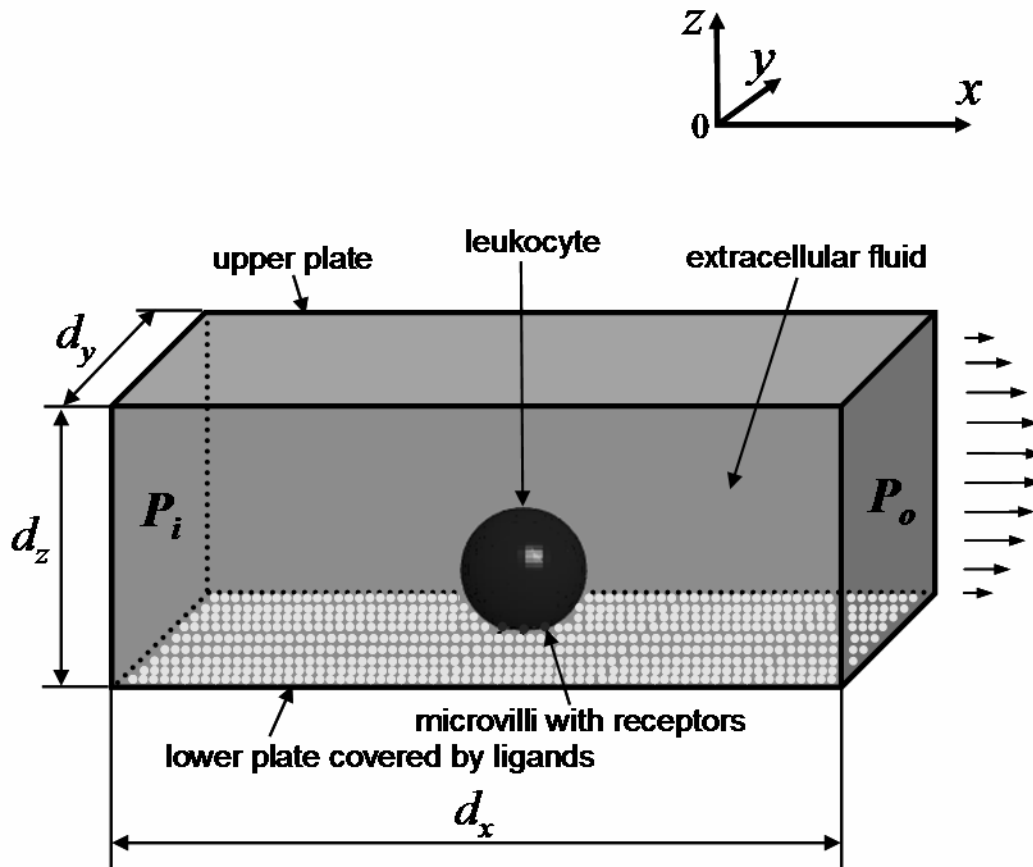


Fig. 3

**MAC grid cell**

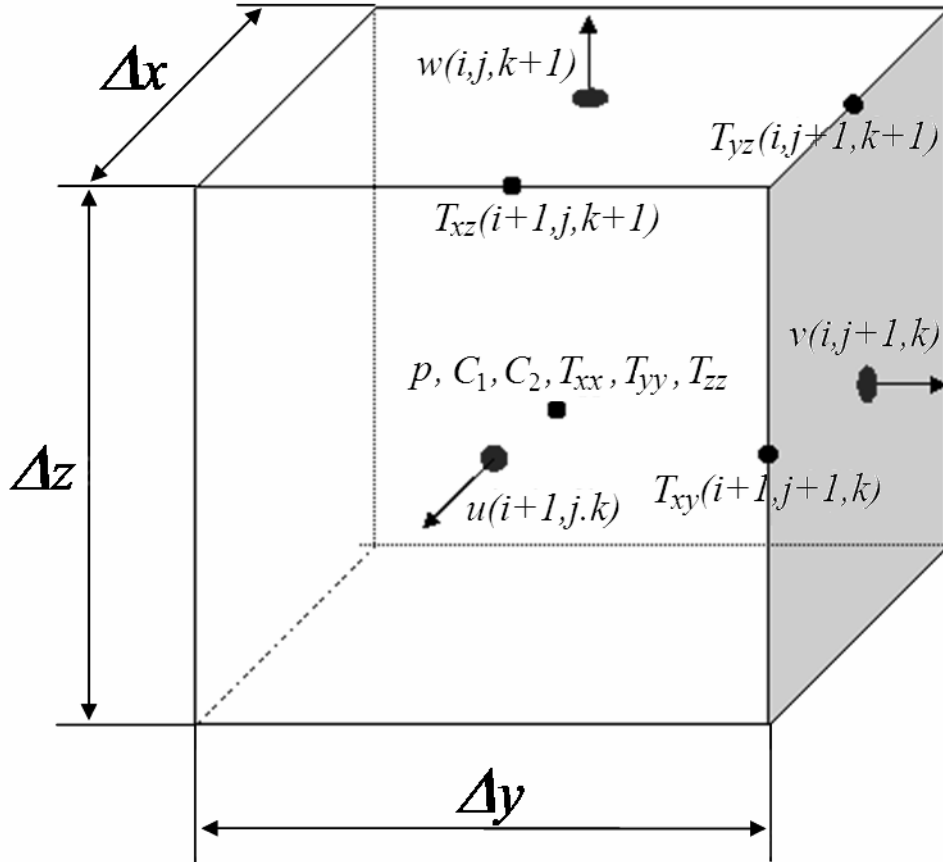


Fig. 4

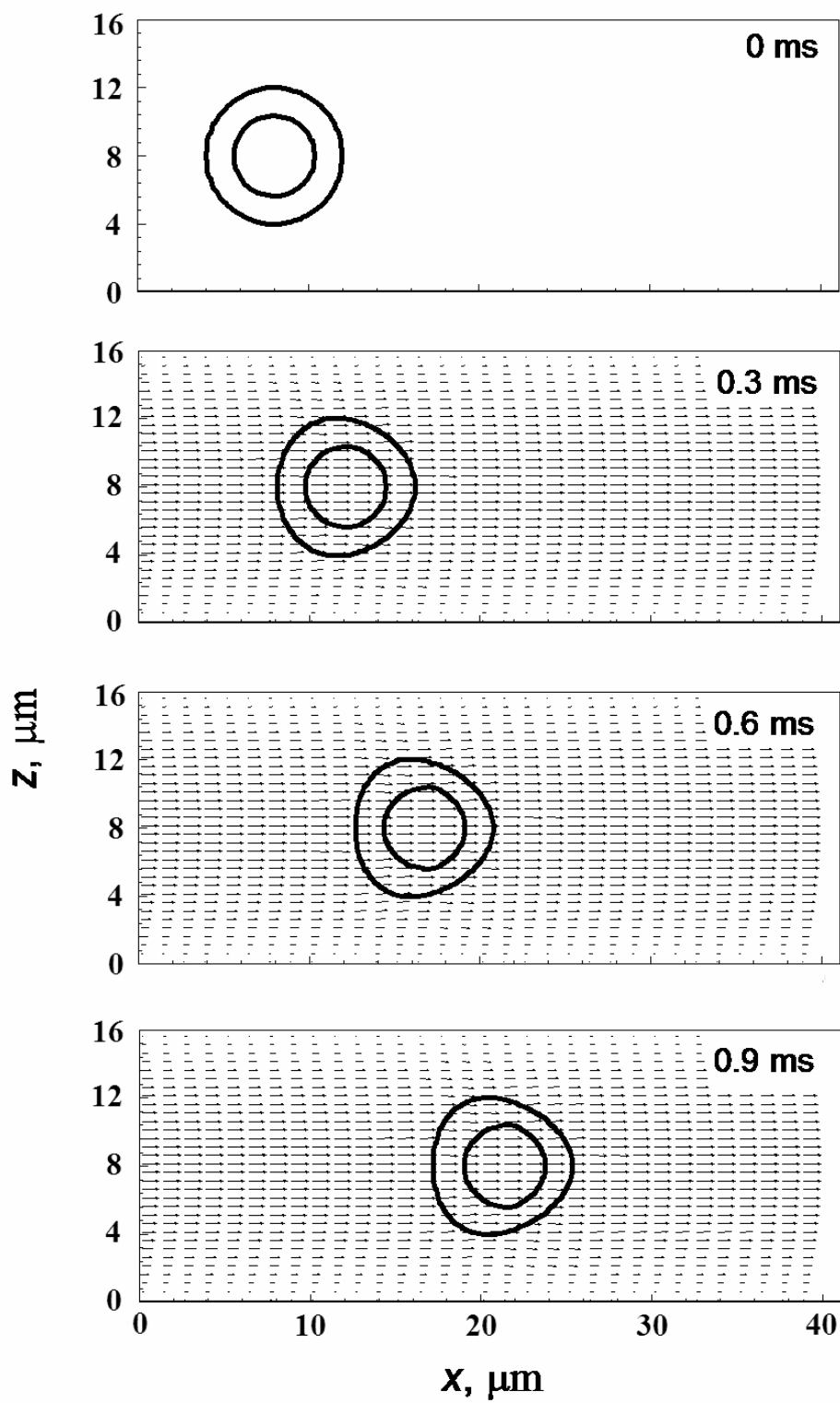


Fig. 5

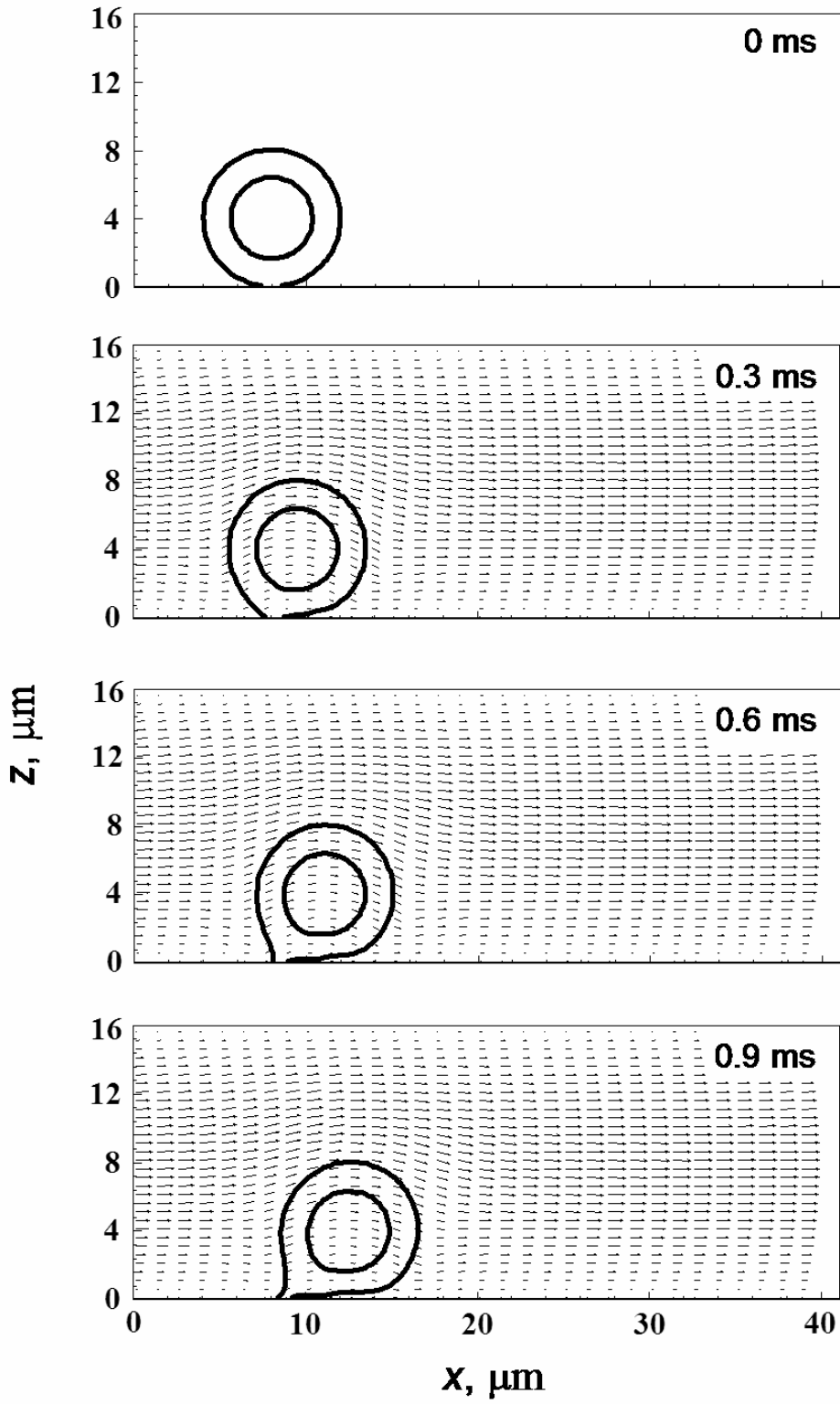


Fig. 6

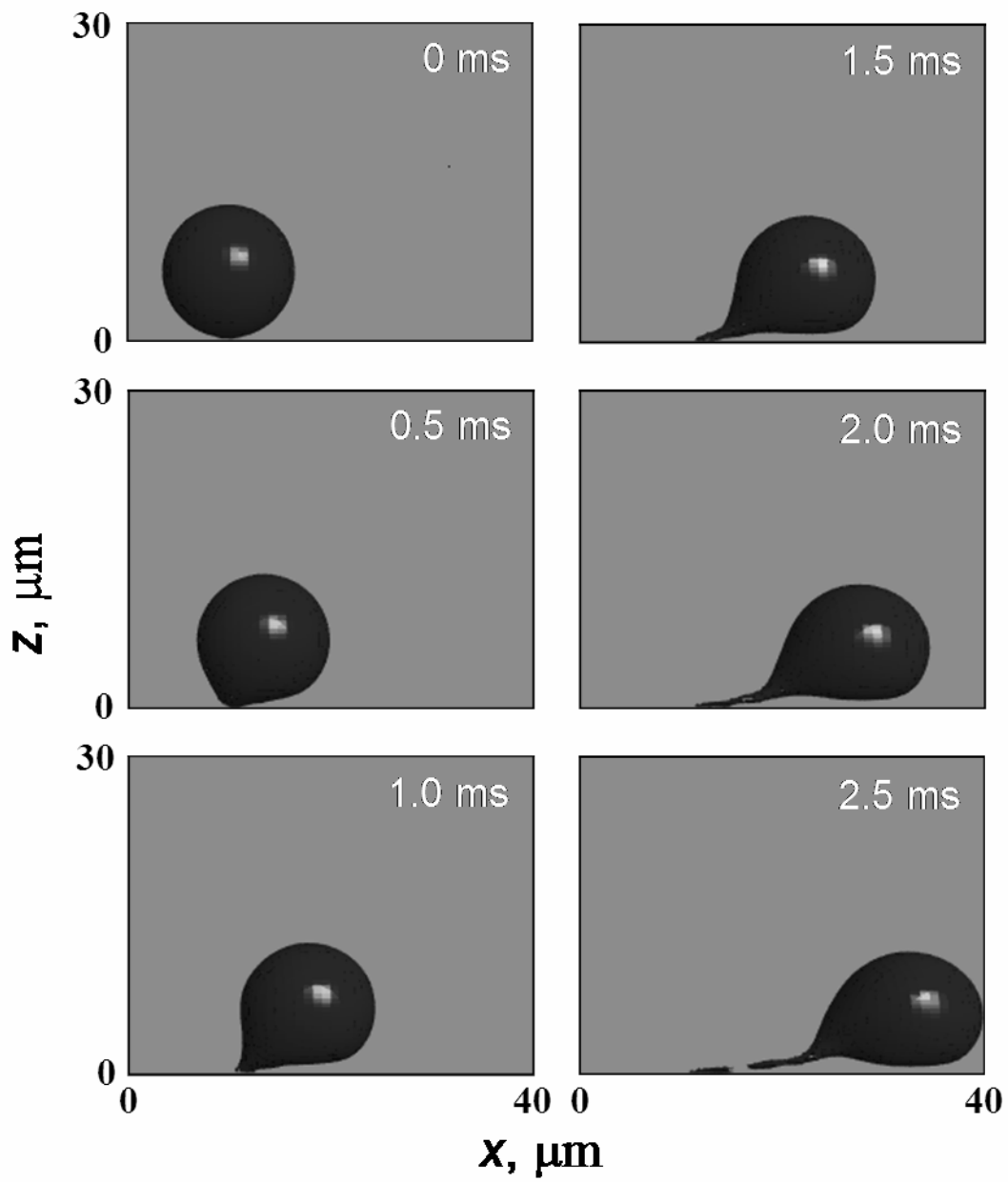


Fig. 7

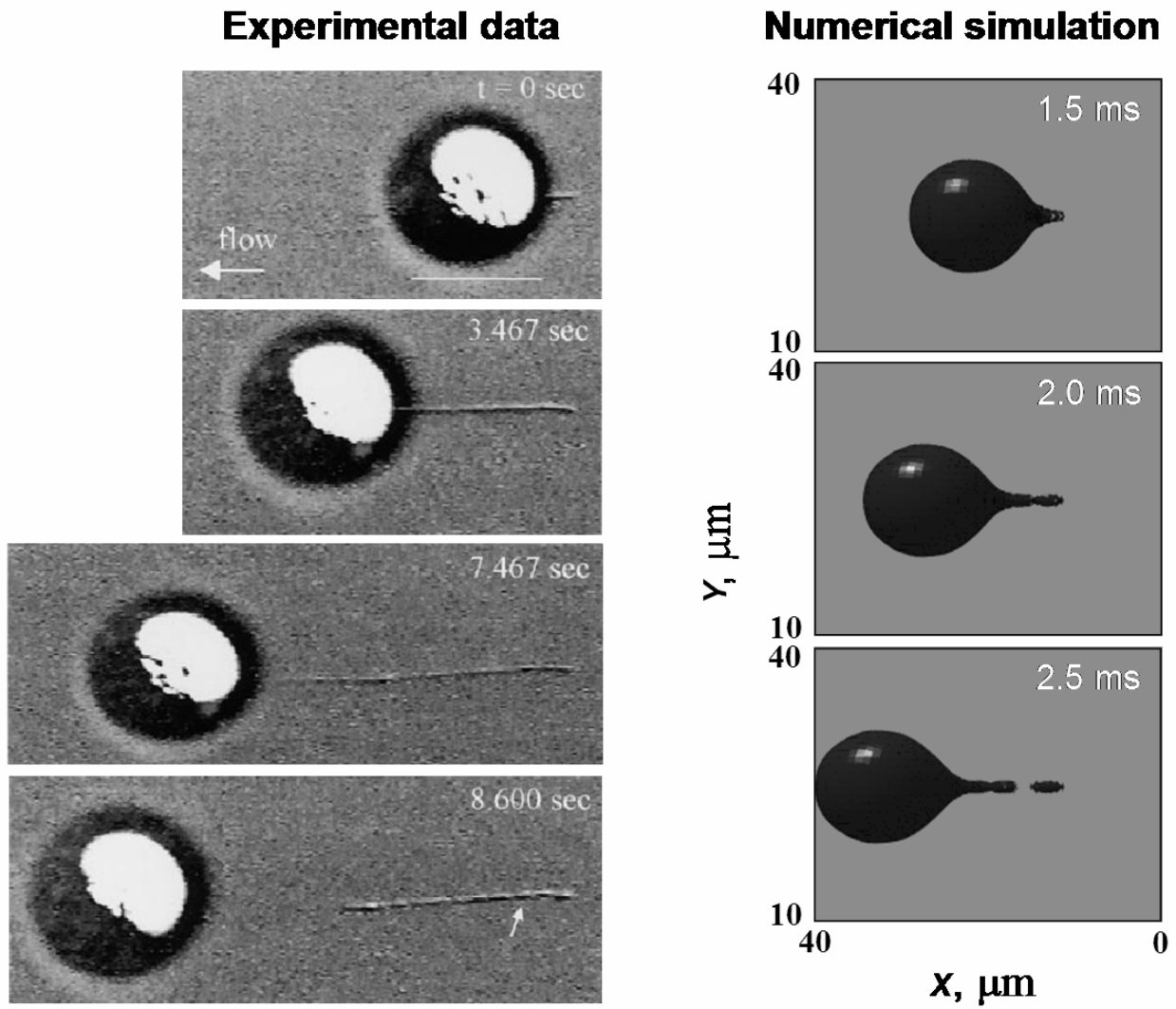


Fig. 8

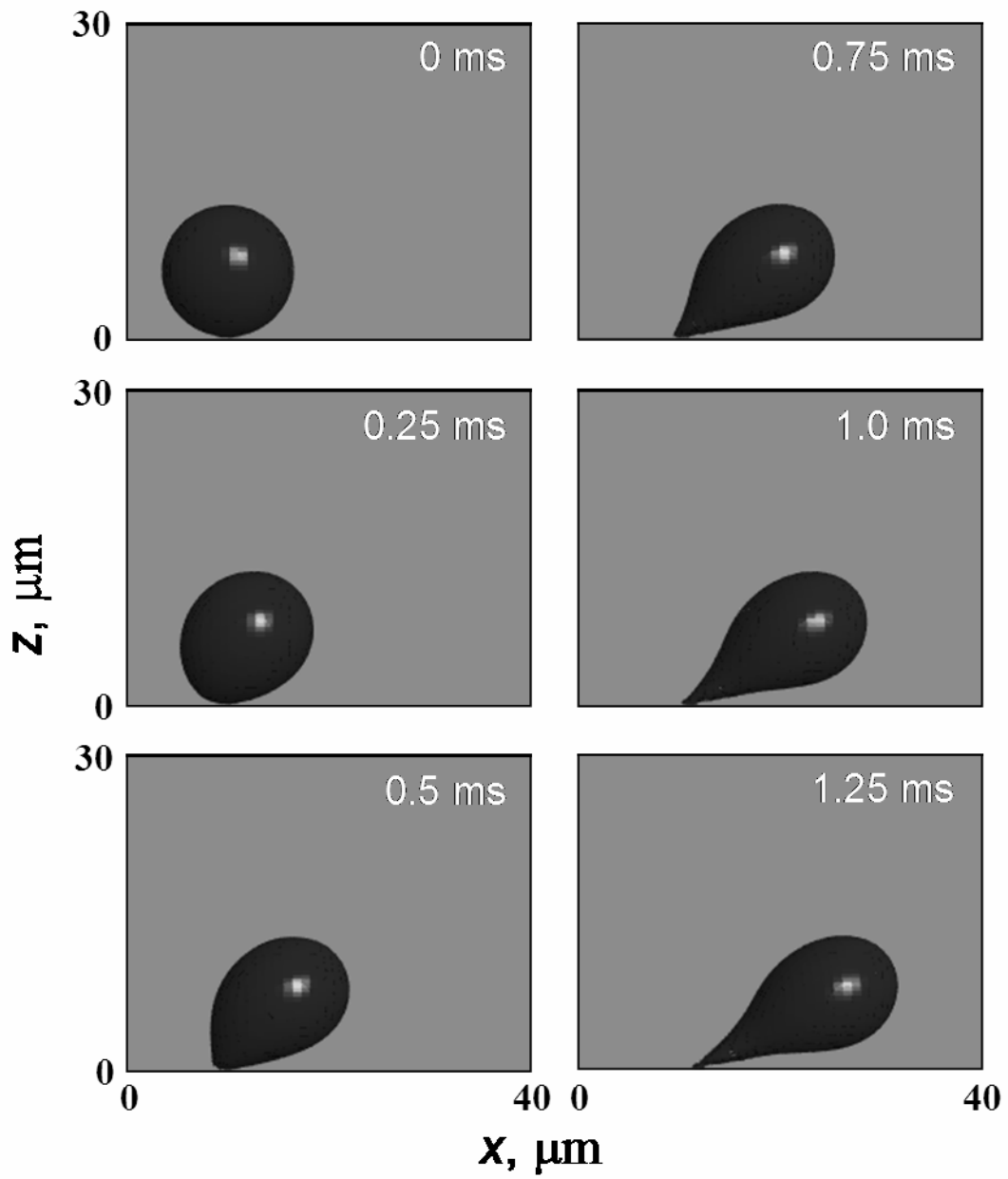


Fig. 9

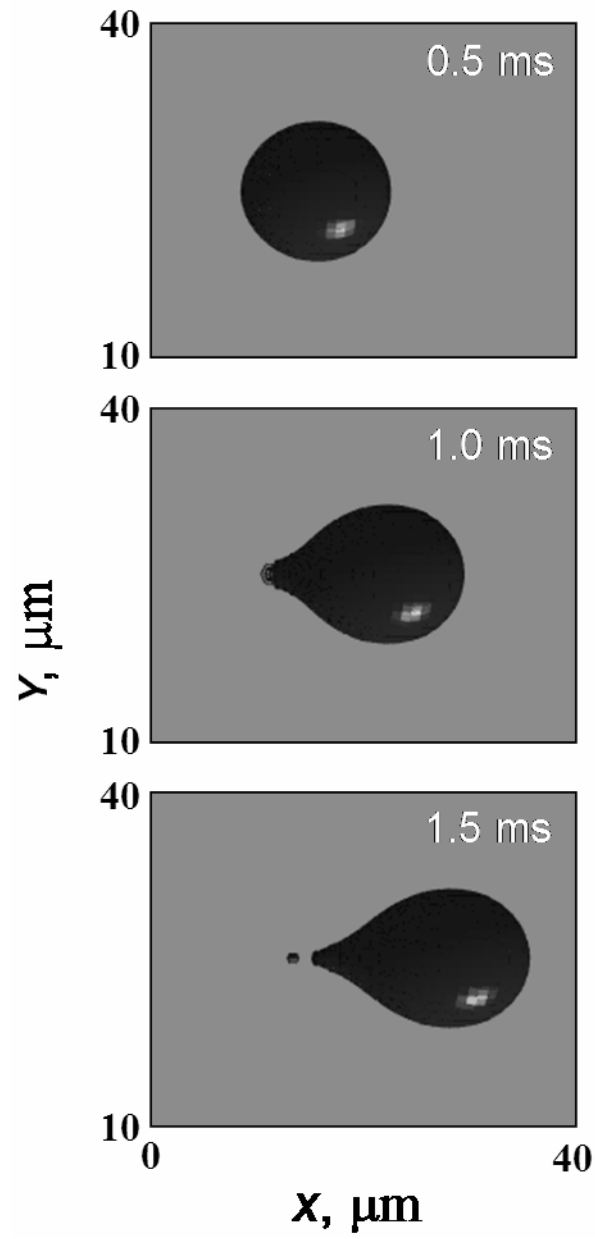
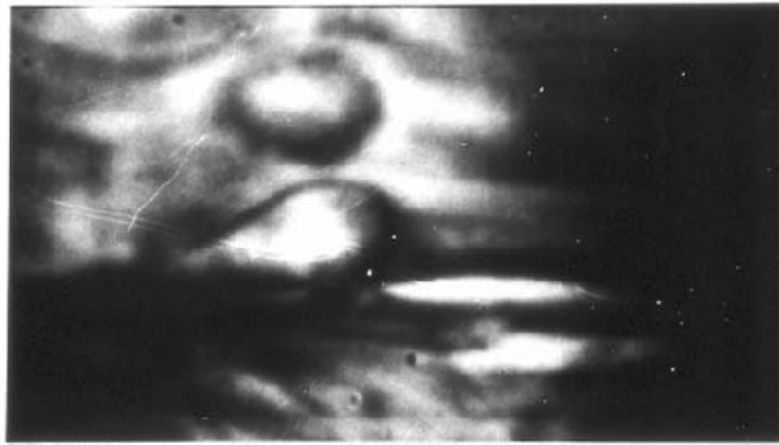


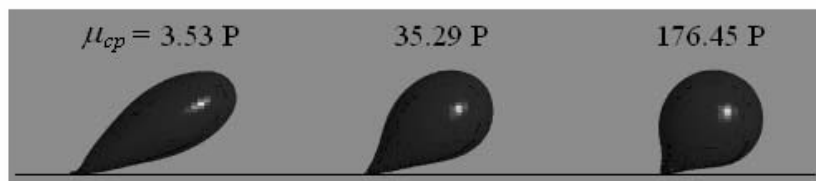
Fig. 10

(a)



10  $\mu\text{m}$

(b)



(c)

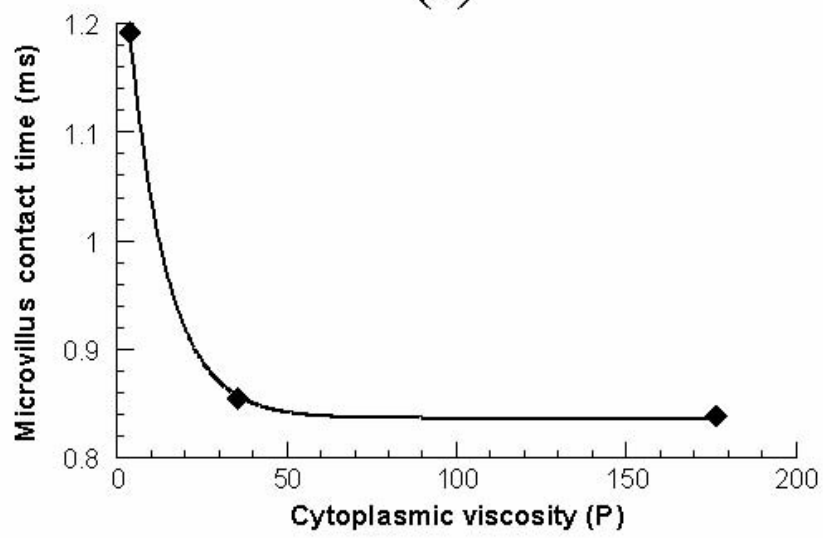


Fig. 11

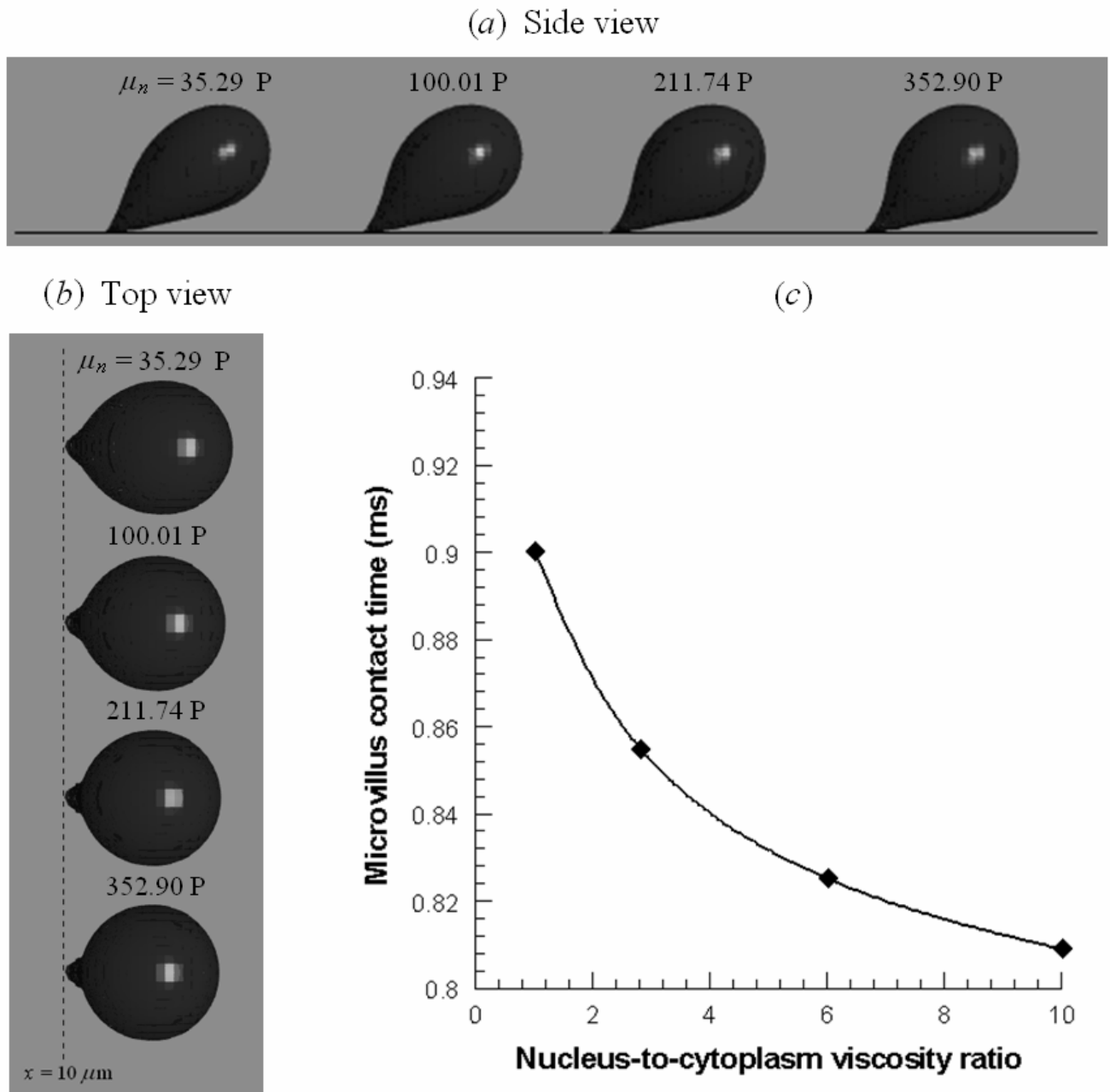


Fig. 12

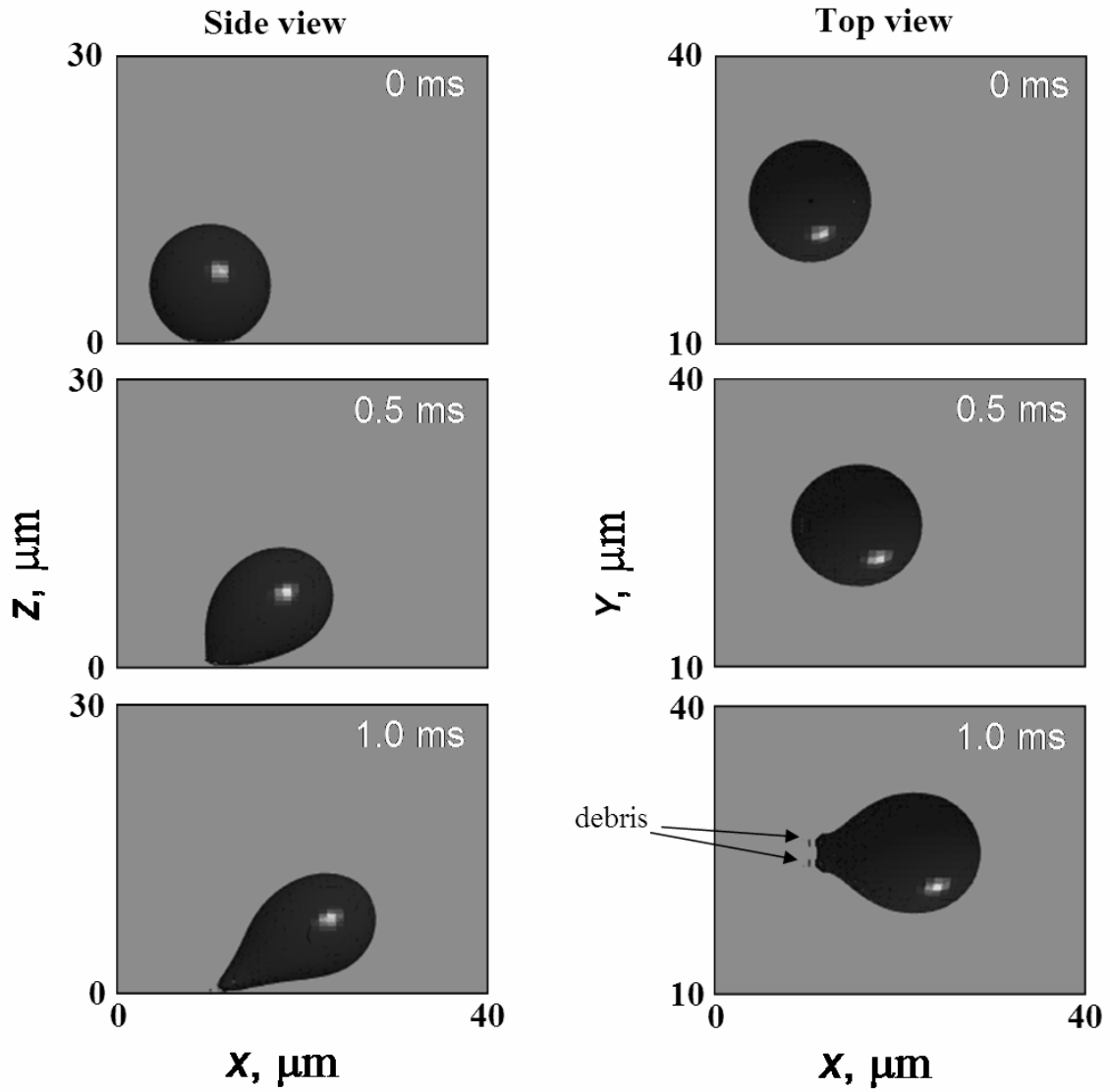


Fig. 13

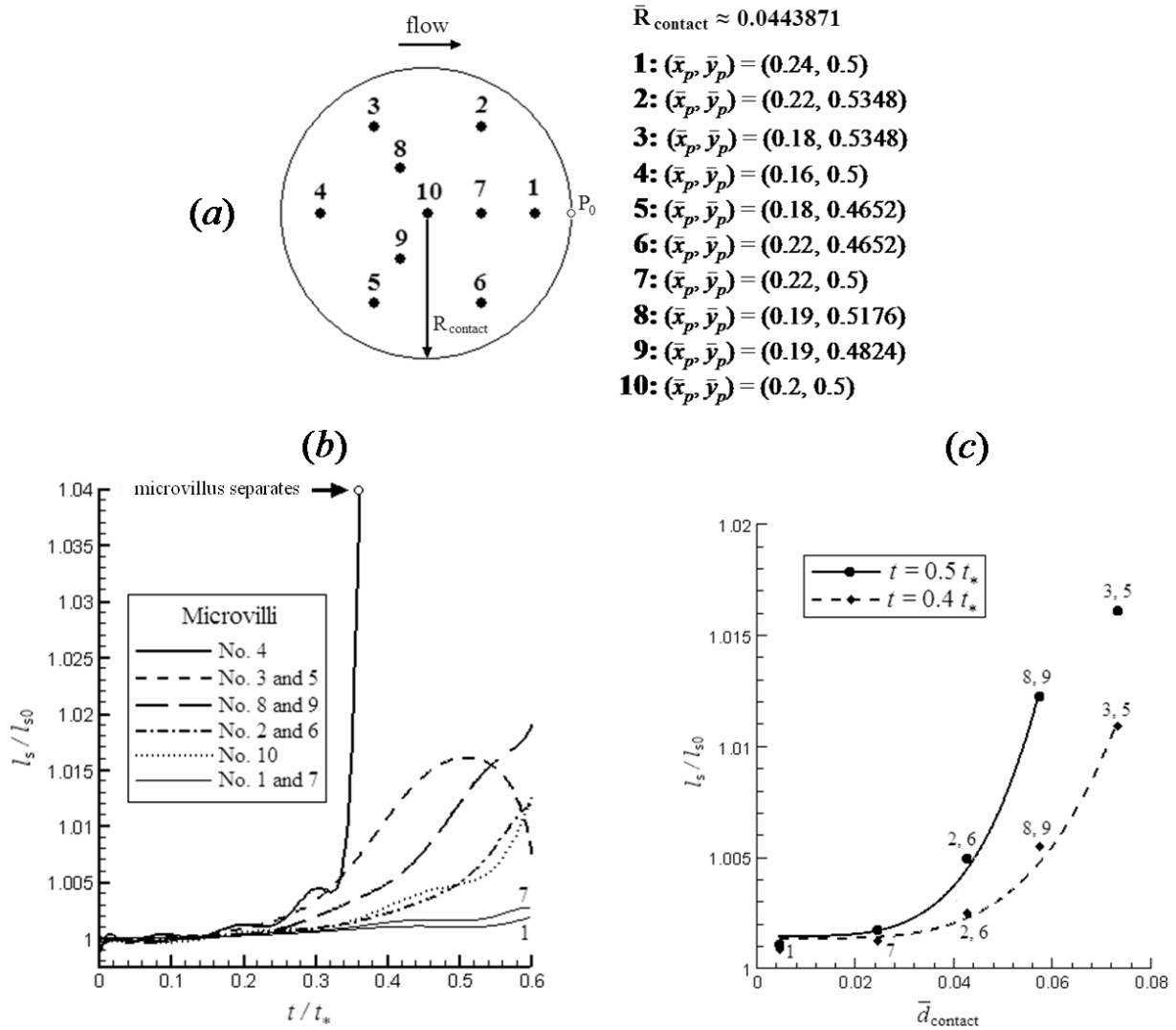


Fig. 14

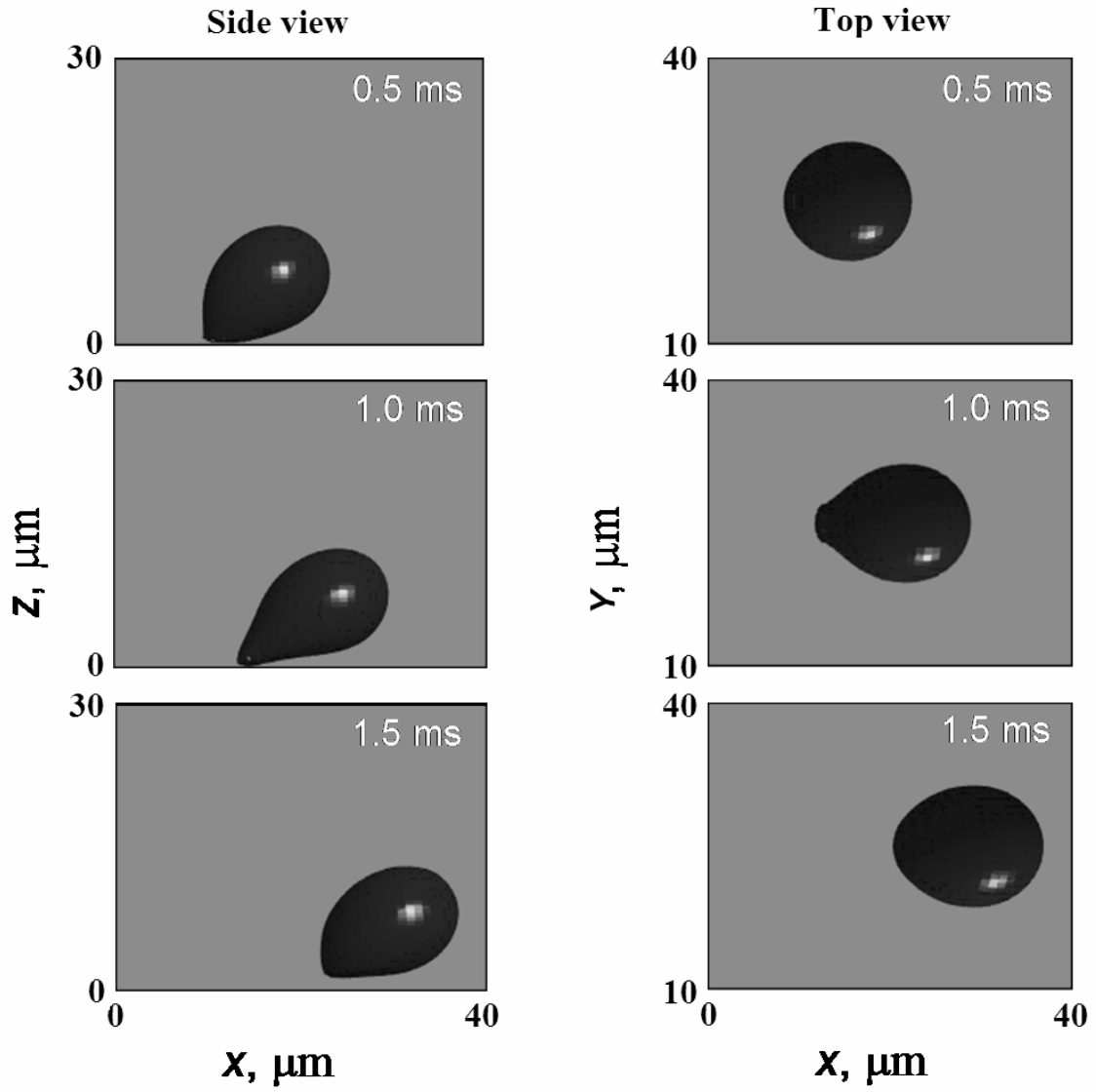


Fig. 15

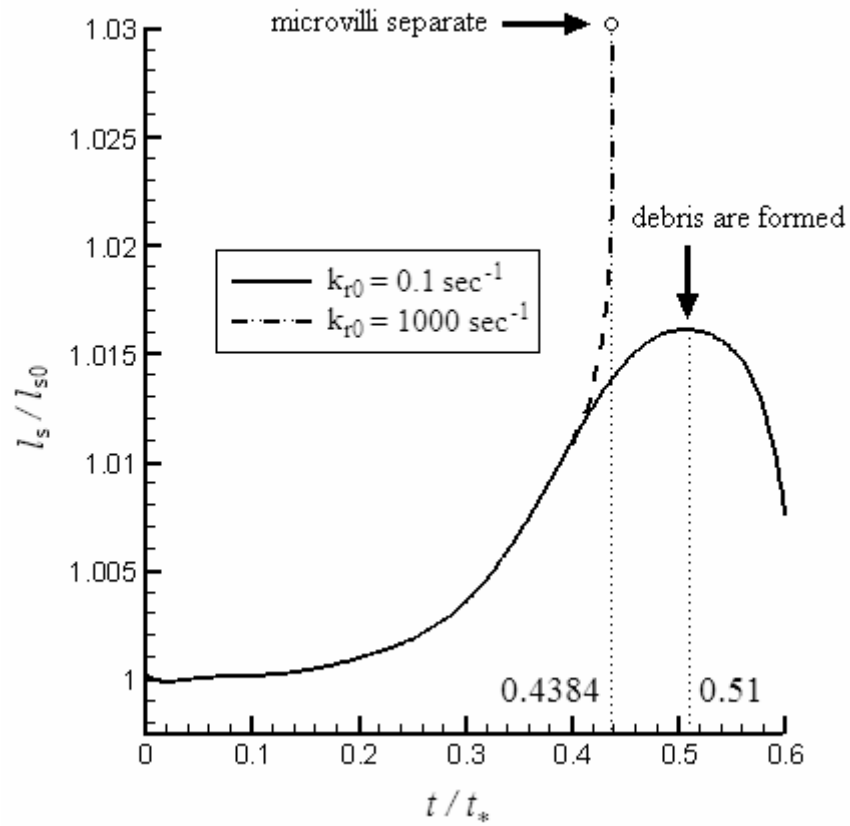


Fig. 16

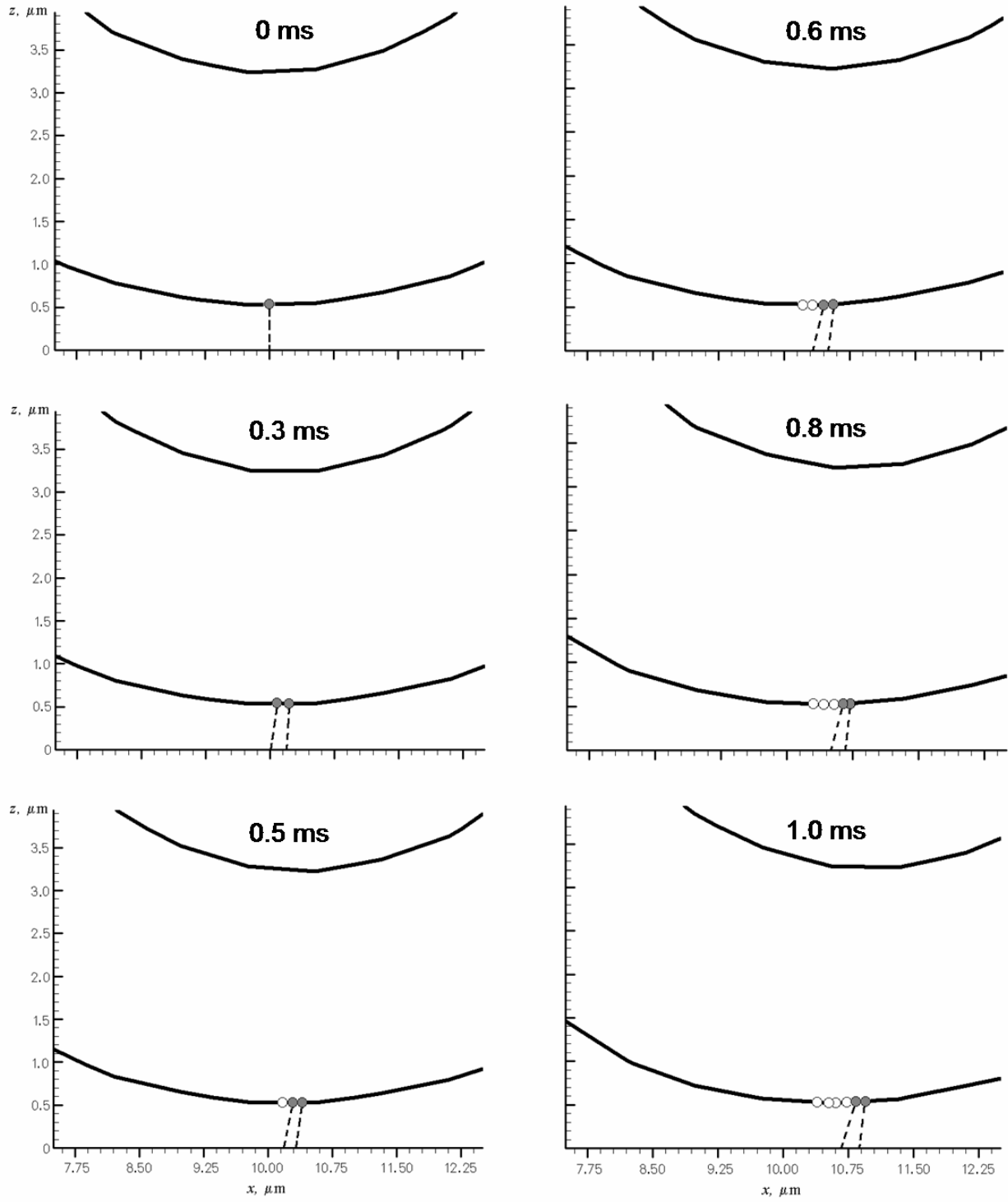


Fig. 17

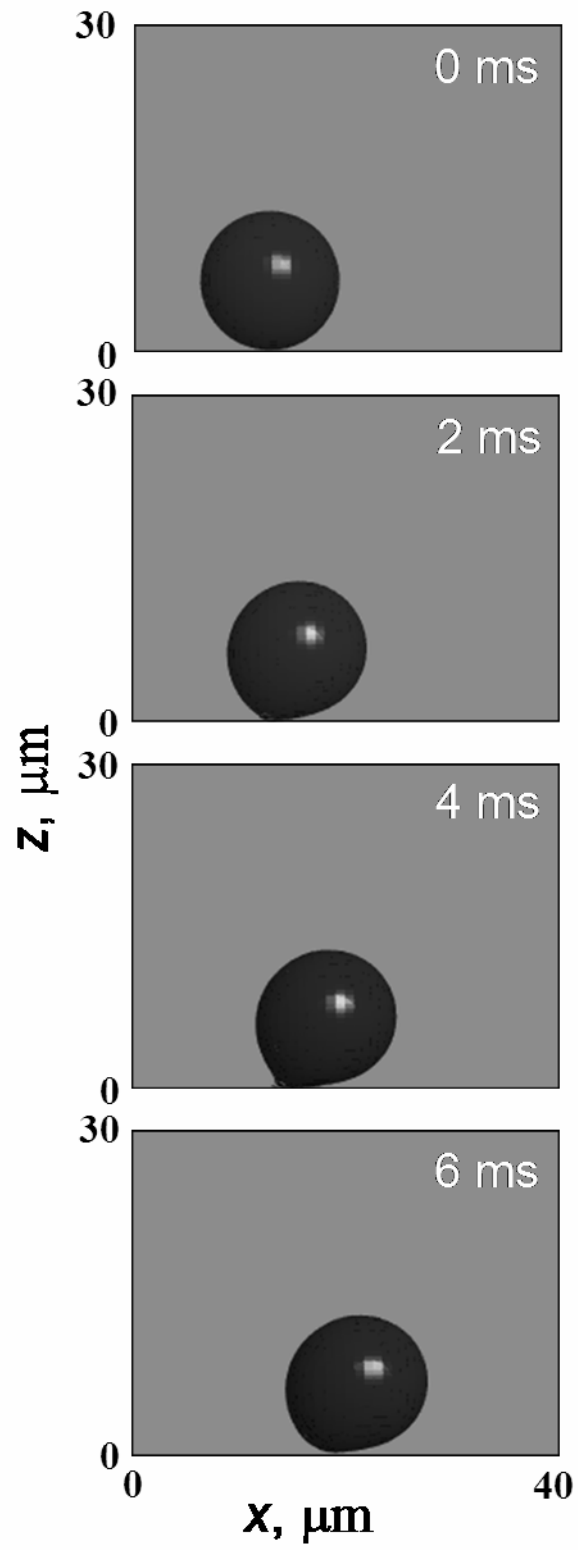


Fig. 18

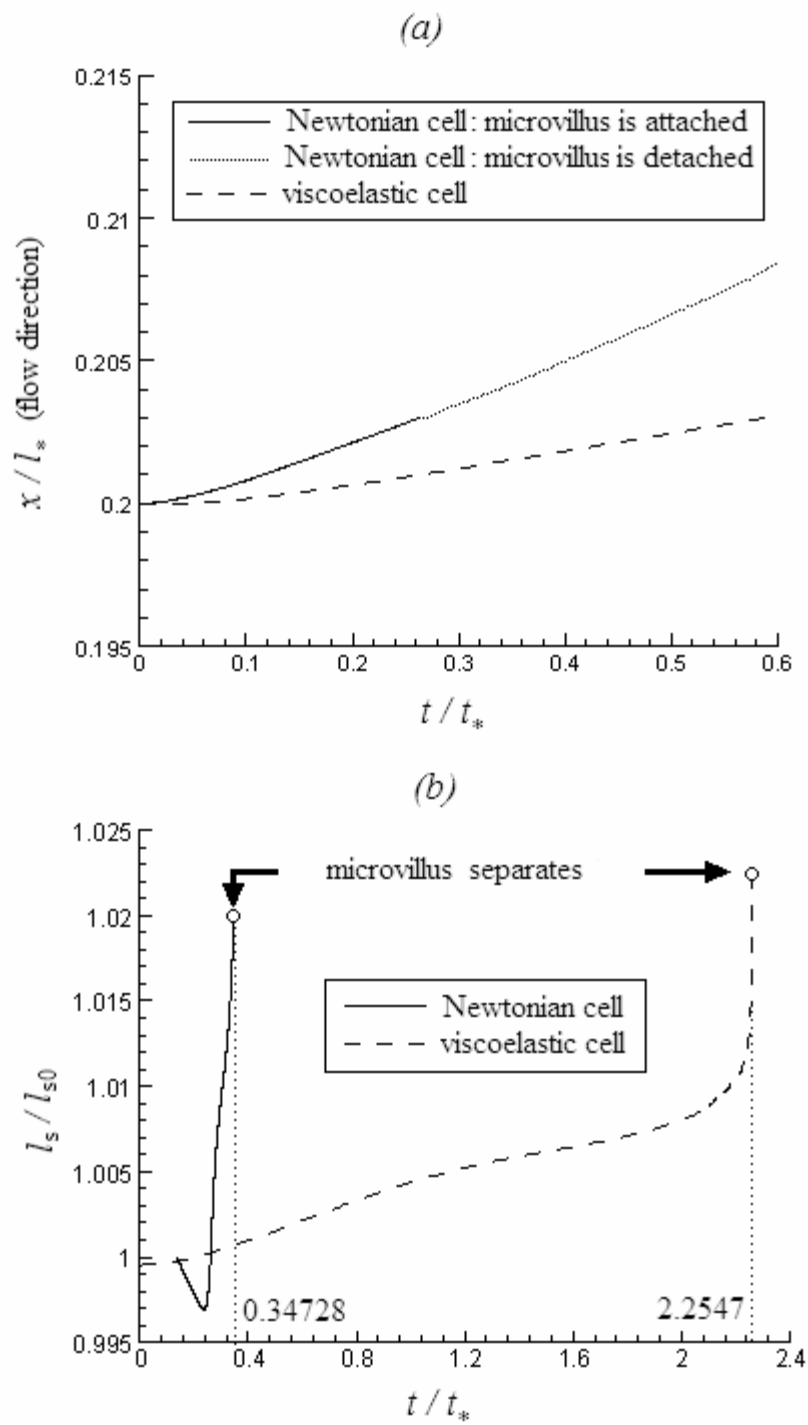


Fig. 19